

Climate change made the extreme 2-day rainfall event associated with flooding in Midleton, Ireland more likely and more intense

Ben Clarke, *Grantham Institute, Imperial College London, UK*

Peter Thorne, *ICARUS Climate Research Centre, Maynooth University, Maynooth, Ireland*

Ciara Ryan, *Met Éireann, Glasnevin, Dublin 9, Ireland*

Mariam Zachariah, *Grantham Institute, Imperial College, London, UK*

Conor Murphy, *ICARUS Climate Research Centre, Maynooth University, Maynooth, Ireland*

Gerard McCarthy, *ICARUS Climate Research Centre, Maynooth University, Maynooth, Ireland*

Paul O'Connor, *ICARUS Climate Research Centre, Maynooth University, Maynooth, Ireland*

Emmanuel O. Eresanya, *ICARUS Climate Research Centre, Maynooth University, Maynooth, Ireland*

Niamh Cahill, *ICARUS Climate Research Centre, Hamilton Institute and Department of Mathematics and Statistics, Maynooth University, Maynooth, Ireland*

Barry Coonan, *Met Éireann, Glasnevin, Dublin 9, Ireland*

Review authors

Friederike Otto, *Grantham Institute, Imperial College London, UK*

Main findings

- On the 17th and 18th October 2023, Storm Babet brought record rainfall amounts to the south of Ireland leading to significant flooding, with the town of Midleton, County Cork severely impacted. The intense 2-day rainfall fell on soils saturated by over 3 months of above average rainfall.
- Peak river flows coincided with a spring low tide, meaning that the river was able to efficiently drain into the sea. Had the event occurred at high tide and/or with substantial storm surge, flooding could have been much more extensive.
- From hydrological modelling, we find that high river flows in October upstream of Midleton are principally driven by extreme rainfall over 2-days and above average preceding rainfall over a longer period (leading to soil saturation), with little evidence of a significant contribution from recent land use changes.
- In order to assess whether and to what extent human-induced climate change was a driver of the rainfall leading to this flood we combine observations-based data products and climate models to look at both the extreme 2-day October and 3-month July-September accumulations over County Cork.

- We find that 2-day October rainfall at least as high as occurred on 17-18th October 2023 has more than doubled in likelihood and increased in intensity by around 13% due to global warming since pre-industrial levels. This result has high confidence with agreement between models and observations. At 2 degrees of warming, there is also high confidence of further increases in the likelihood and intensity of such events. However, these projected changes are challenging to quantify due to model uncertainties, and so the reported results of a 20% increase in likelihood and 2% in intensity have low confidence.
- On the other hand, the observed high antecedent rainfall from July-September may have become less likely by about 25% and the rainfall totals have reduced by around 5%. However, this result has very low confidence due to high uncertainties across all datasets and the disagreement in the direction of change between models (drying) and observations (wetting).
- In summary, forensic analysis of the drivers of flooding in Midleton show that changes in extreme rainfall due to anthropogenic climate change drove more intense flooding in October 2023, and such changes are likely to continue with further warming. Despite the substantial damages, Midleton proverbially ‘dodged a bullet’ of a far worse disaster thanks to the chance spring low tide at the time of the peak river flow.

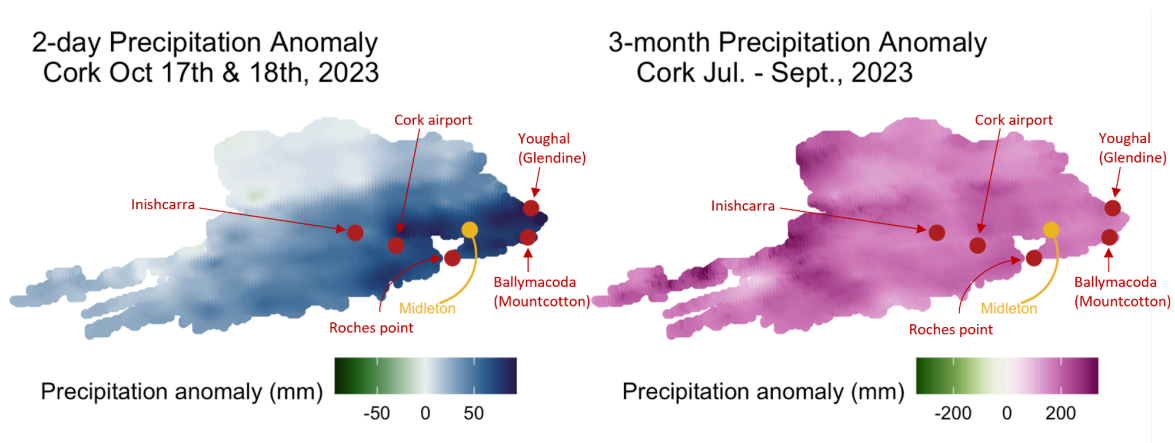


Figure H1: Rainfall anomalies for County Cork from the Met Éireann gridded product, showing the 2 days of Storm Babet (left) and July-September accumulations (right), each versus the 1980-2010 average for the same period and event type. In and around Midleton (SE County Cork) many areas received in excess of 100 mm of rainfall in two days due to Storm Babet, while the entire county received significantly above average rainfall for the preceding months.

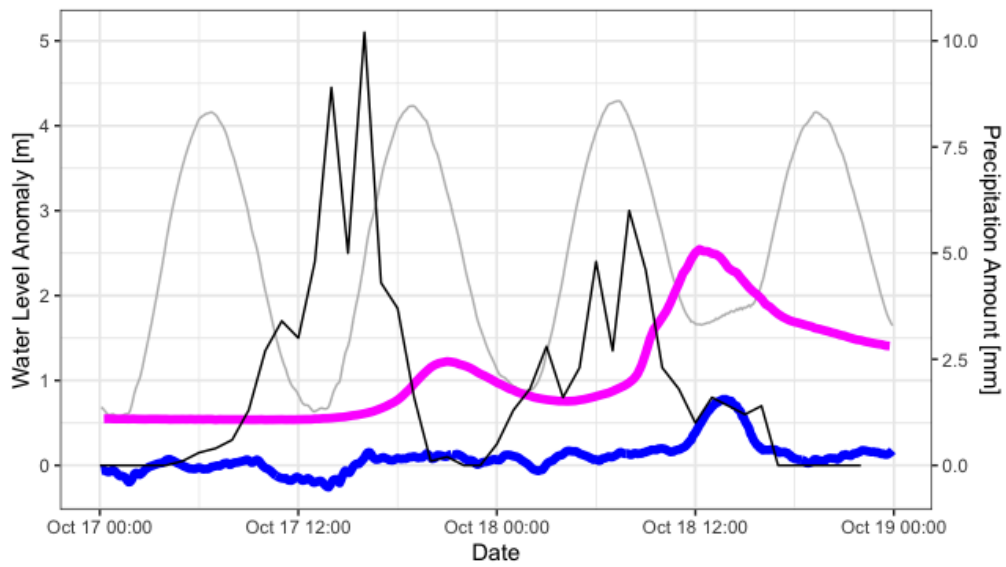


Figure H2: Hourly precipitation recorded at Roches Point meteorological station (black). Water level anomaly recorded at the Owenacurra river gauge at Ballyedmond (magenta), full water level (grey) and non-tidal residuals (blue) recorded at Bailick Road tidal station. See Figure 4 in main text for locations.

1 Introduction

1.1 Context

On 18th October 2023, the town of Midleton, County Cork, Ireland witnessed significant and damaging fluvial flooding associated with storm Babet ([RTE, 2023a](#), [Arup, 2023a,b](#)). The event was caused by extreme 2-day rainfall amounts which followed a sustained period of anomalously wet weather that started with the wettest July on record nationally. Three Cork based stations had their wettest October on record. Roches Point observed 222% of its long-term average, breaking a record which extends back over 140 years (Figure 1). By the end of October, Cork Airport, Roches Point, and Moore Park, had already observed at or over 100% of their annual average rainfall for 2023 with two months remaining. Anomalously high October rainfall totals were widespread across southern Ireland for the month with the highest anomalies as a percentage of the long-term average centred around County Cork in the vicinity of Midleton (Figure 2).

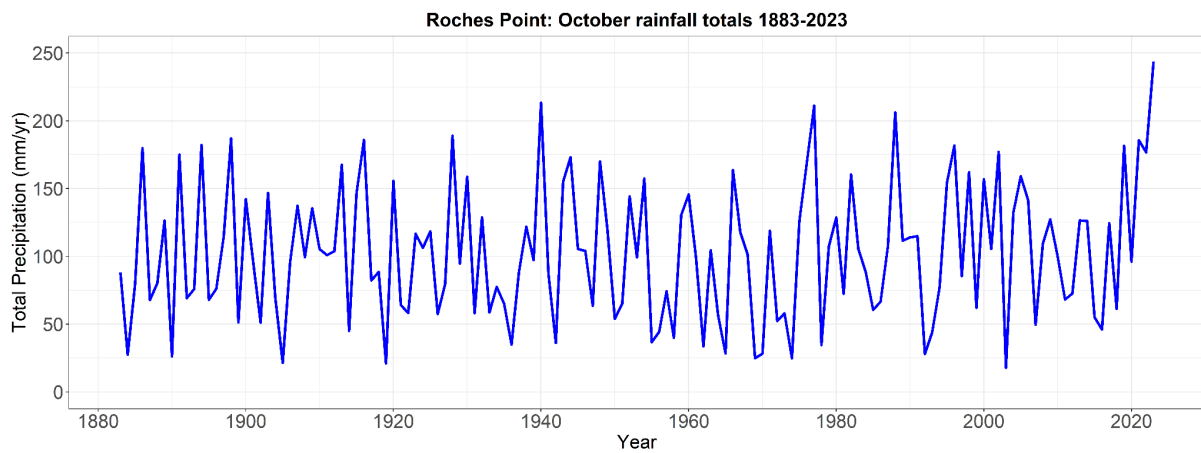


Figure 1: Roches Point October total precipitation since the late 19th Century. 2023 constituted the wettest October on record for this station. Sourced from Met Éireann.

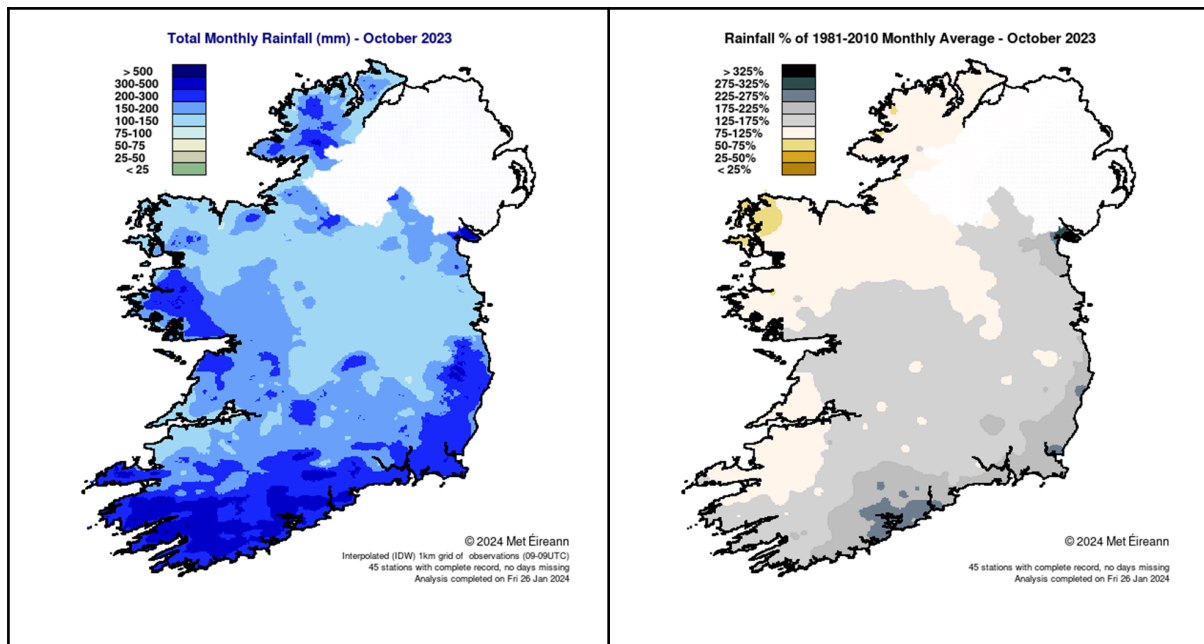


Figure 2: Absolute monthly precipitation totals (left) and departures from climatology as a percentage of the long-term average (right) for the month of October 2023. Sourced from Met Éireann.

Storm Babet led to fluvial flooding in a number of towns in County Cork. The worst affected towns were Midleton, Killeagh, Glanmire and Blackpool. Areas of Cork City were also subject to pluvial flooding during the event (Arup, 2023a). Storm Babet flooding in Midleton thankfully claimed no lives despite the fast arrival of flood waters in the town. There was, however, substantial flood damage to properties and infrastructure across the town (Arup, 2023a,b). A total of 681 properties consisting of 395 residential properties and 286 commercial properties were impacted by flooding (Arup, 2023b). In many cases, peak flood waters at these properties exceeded 1 m depth, particularly in the upstream reaches of Midleton (Arup, 2023a,b). A number of estimates available within a month put the costs of damage to homes, businesses, roads, bridges and other infrastructure at between €150m and €200m (RTE, 2023b). Many of these properties were not insured for flooding following prior flooding events meaning that commercial insurance was not available and / or affordable. A significant fund was made available from central government to support impacted households and businesses. Within the week ‘officials had said that an existing humanitarian scheme to provide relief for businesses ravaged by the floods would be “stood up with quick payments of €5,000 and assessed and audited payments of up to €20,000”. Another exceptional scheme had also been approved for businesses hit by the floods and which have greater levels of damage. Officials said there would be “quick payments of €10,000 and audited and assessed payments of up to €100,000” under this second scheme.’ (Irish Times, 2023a). Supports were subsequently extended again (RTE 2023c).

1.2 Event evolution

Heavy precipitation was recorded at the meteorological station at Roches Point, 13 km southwest of Midleton, on 17th of October with hourly values peaking above 10 mm (Figure 3). Increases in water level were recorded at the river gauge at Ballyedmond (gauge number 19020, Table 1 and Figure 4) at the outlet of the Owenacurra catchment late on the 17th, with waters returning to near normal levels

overnight. Further heavy rainfall was recorded on the 18th. Water levels rose rapidly at the Ballyedmond river gauge on the 18th. Water levels peaked at 2.54 m above normal levels at 12:15 on the 18th based upon 15-minute resolution reports. These were the highest levels recorded at this gauge since June 1977 when the record began, resulting in the damaging floods in Middleton¹.

The water level gauge at Bailick Road (station number 19166, Table 1 and Figure 4) is downstream of Middleton and the confluence of the Owenacurra and Dungourney rivers and is a tidal location. Low tide was due at 13:25 on the 18th of October. Non-tidal residuals at Bailick Road peaked at 0.78 m at 13:50 indicating the large discharge of the floods from the Owenacurra and Dungourney rivers. Non-tidal residuals returned to normal levels rapidly, with no excess water recorded at high tide at 19:20. Levels at the Ballyedmond river gauge remained elevated in the following days.

Another peak in precipitation was recorded on October 20th that resulted in elevated water levels at Ballyedmond. This event on the 20th of October was in the top 6 events recorded by the gauge but did not result in significant flooding at Middleton.

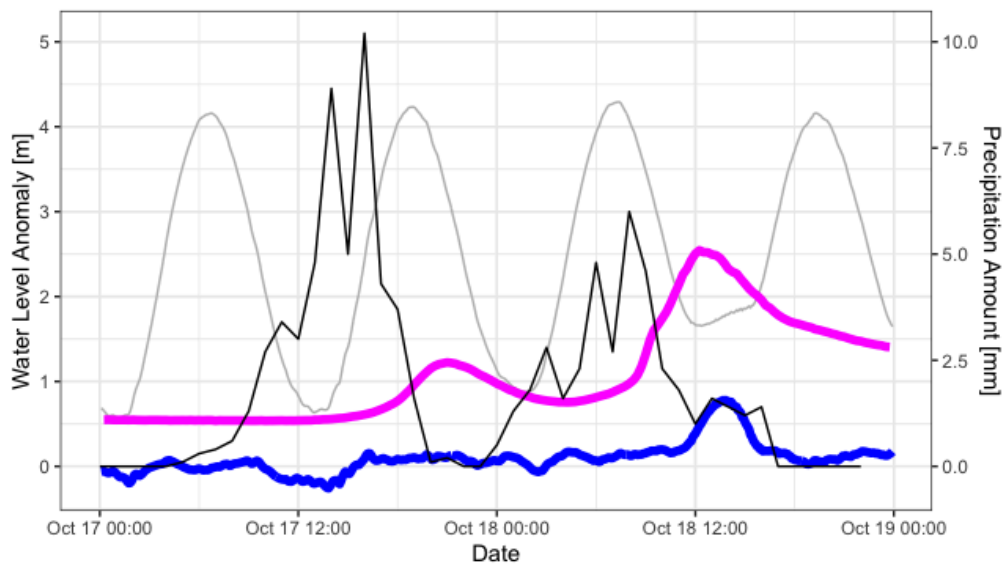


Figure 3: Hourly precipitation recorded at Roches Point meteorological station (black). Water level anomaly recorded at the Owenacurra river gauge at Ballyedmond (magenta), full water level (grey) and non-tidal residuals (blue) recorded at Bailick Road tidal station. See Figure 4 for locations.

| Station | Name | Lat (°S) | Lon (°E) | Maximum non-tidal water level anomaly (m) | Time of maximum level On 18 th October 2023 |
|---------|--------------|----------|----------|-------------------------------------------|--------------------------------------------------------|
| 1. | Ballyedmond | 51.94 | -8.20 | 2.54 | 12.15 |
| 2. | Bailick Road | 51.90 | -8.17 | 0.78 | 13.50 |

¹ Note that data at the gauge is discontinuous until early 2000 and there was a hiatus in the measurement series from April 2014 until March 2017 which includes the stormiest (2014/15) and wettest (2015/16) winters on record nationally ([Matthews et al. \(2014\)](#); [Murphy \(2018\)](#); [Matthews et al. \(2018\)](#)). It is therefore possible that higher values occurred within the period of record but were not recorded.

Table 1. Spatial coordinates and maximum water levels for selected water level stations.

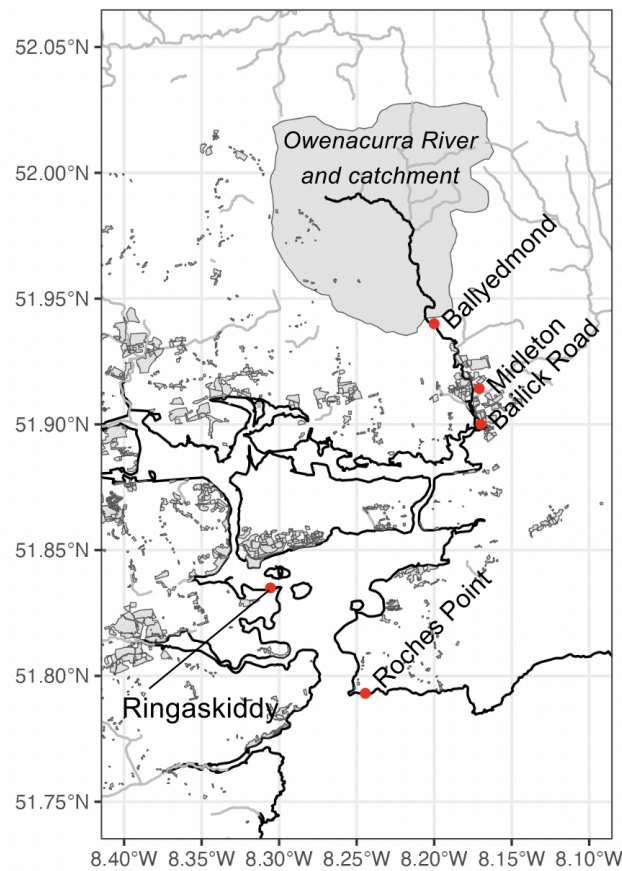


Figure 4: Locations mentioned in the text. Owenacurra River and Catchment. Other rivers are also shown in grey. The town of Midleton is shown with the location of residential and commercial properties. Water level and flow gauges upstream of Midleton at Ballyedmond and the water level gauge downstream of Midleton at the tidal Bailick Road are shown. Tide gauge station at Ringaskiddy and the Synoptic Meteorological Station at Roches Point are also shown. See text for references to these various locations throughout.

Extratropical storms are a common occurrence at this time of year in this region. However, storms bringing as much precipitation as storm Babet did are much rarer. Synoptically, the storm event arose from a complex depression of sub-tropical origin which drifted slowly up from off the Iberian peninsula to become centred over the British and Irish isles over the period 16th-19th October 2023 (Figure 5). Within this depression were very high total precipitable water values reflecting the storm's origin over very warm subtropical Atlantic waters, widely in excess of 30mm and in parts in excess of 50mm (Figure 6 and Figure S1). This resulted in widespread high precipitation totals and associated impacts over many parts of the British and Irish isles over this period ([JBA, 2023](#)).

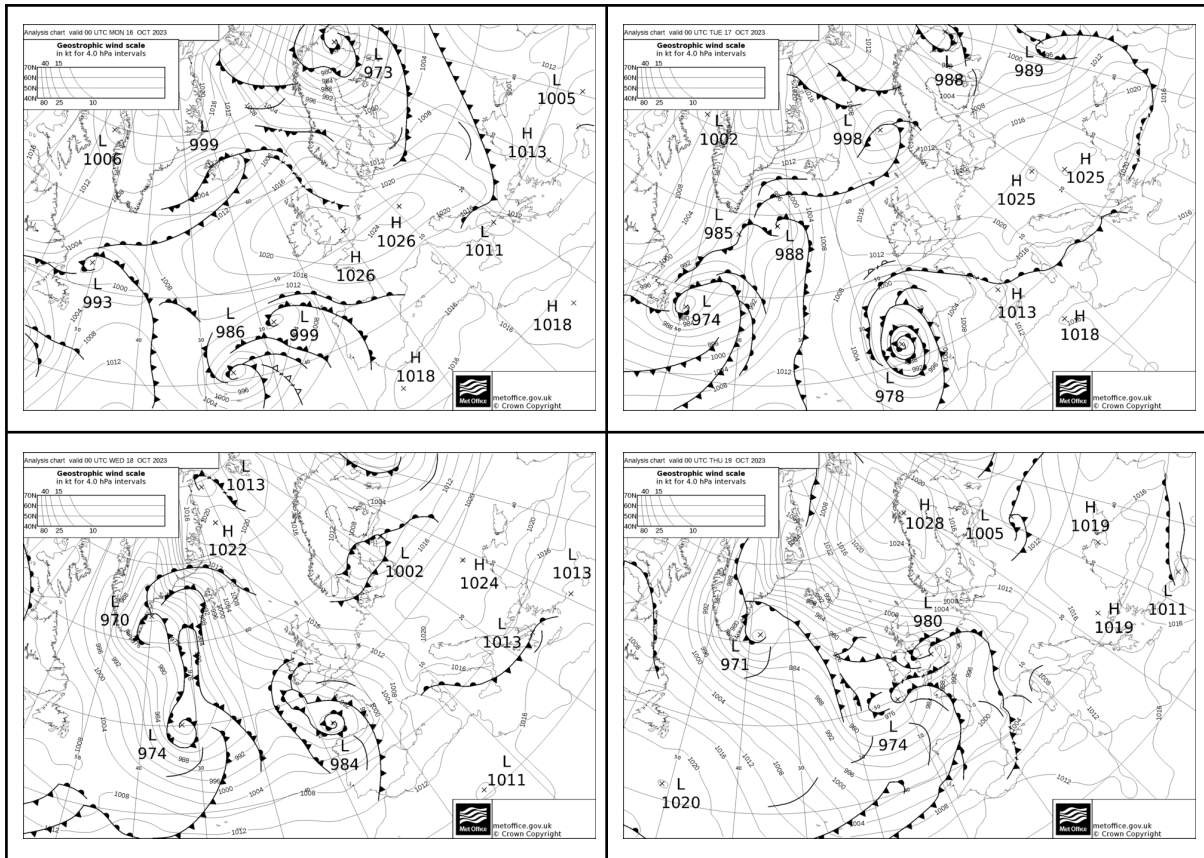


Figure 5. Synoptic evolution of storm Babet over the period of 16th-19th October 2023 based upon 00 UTC synoptic analyses undertaken by the UK Met office.

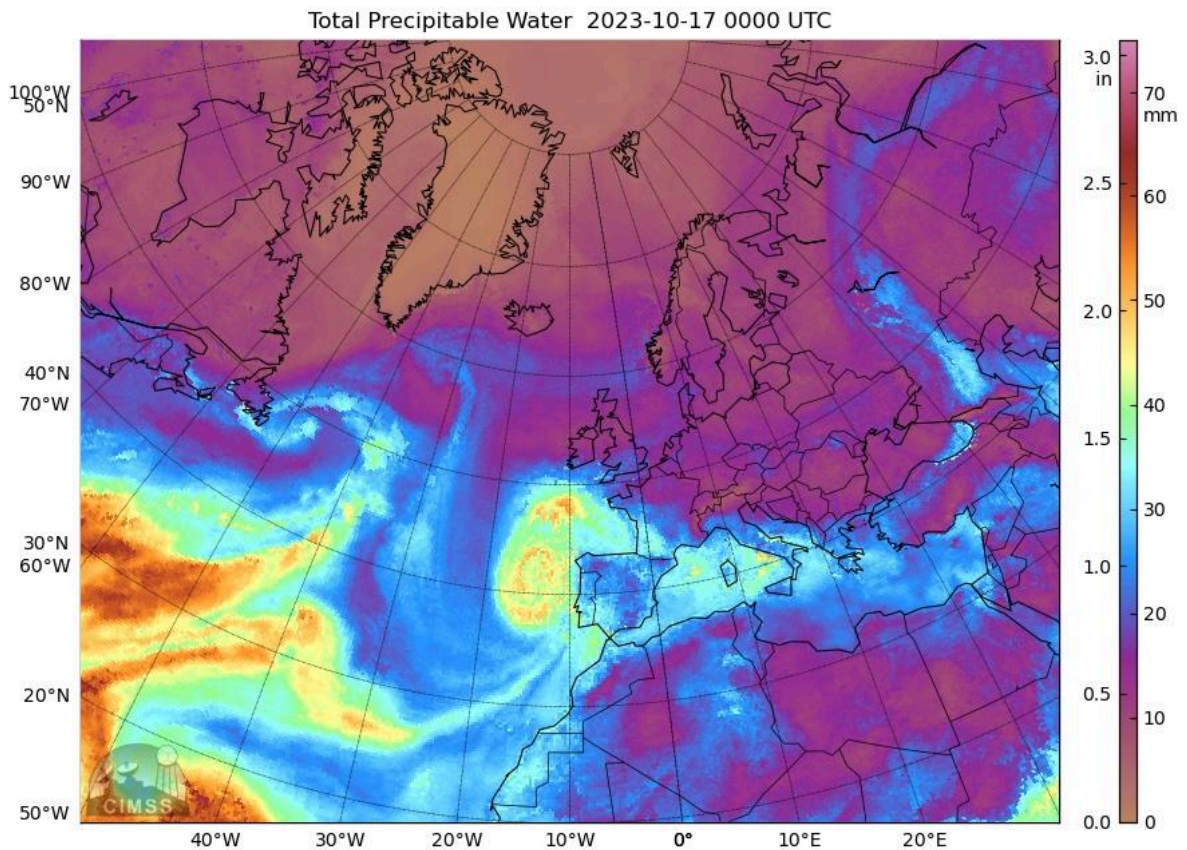


Figure 6. Total Precipitable Water (TPW) from 00 UTC on 17/10/23. Storm Babet at this point is approaching Ireland from the south and is present as an elevated region of TPW centred to the west of the Iberian peninsula (c.f. Figure 5 second panel). The 6 hourly snapshots of TPW estimates from 00 UTC on 16/10/23 until 18 UTC on 18/10/23 covering the period of the analysis herein and highlighting the evolution of TPW are given in Figure S1. Sourced from the [MIMIC-TPW2 product](#) from CIMMS, University of Wisconsin-Madison.

1.3 Attribution to anthropogenic climate change

Extreme weather attribution (henceforth attribution) is a suite of methods that help to answer the question of whether and to what degree anthropogenic climate change affected the likelihood and intensity of a given extreme event ([Otto et al., 2017](#), [Leach et al., 2021](#)). This is often calculated for the event at the time of occurrence, and for similar events at given hypothetical global warming levels ([Philip et al., 2020](#)). In doing so, attribution provides both a snapshot of the current hazard and a trajectory of changes due to climate change ([van Oldenborgh et al., 2021](#)).

Increasingly, attribution studies are based on the aspect(s) of the weather that most directly led to impacts on communities and property, rather than the most extreme aspects or those with the strongest expected connection to climate change ([van Oldenborgh et al., 2021](#)). As a result, these studies can provide a number of benefits. First, they highlight where the relatively abstract phenomenon of global warming is leading to increasing hazards, and where it is having little effect or reducing certain hazards. This is a useful consideration for informing an accurate perception of climate change and its effects to date ([Ettinger et al., 2021](#)), adding another line of evidence to nuanced discussions and balancing resources for both mitigation and adaptation ([Stott et al., 2016](#)). On the latter, attribution studies also provide a direct assessment of changing hazards based on events that occurred and are therefore known to be plausible ([Frame et al., 2020](#)). By then considering exposure and vulnerability of those affected, and the other drivers of these, a more complete picture can be built that is directly applicable to managing risks ([Otto, 2023](#)).

Hundreds of attribution studies exist for events all around the world (e.g. [Herring et al., 2022](#)). Taken together, this constitutes a growing body of evidence on the complex and changing landscape of extreme weather hazards ([Clarke et al., 2023](#); [Carbon Brief, 2022](#)). However, to date, no attribution studies exist for extreme events in Ireland using modern WWA techniques², despite the occurrence of several damaging events including floods arising from: i) long duration precipitation events e.g. River Shannon December 2015 ([RTE, 2015](#)); ii) intense short duration events e.g. Donegal August 2017 ([Irish Times, 2017](#)); iii) groundwater related Turlough flooding in unique karstic landscapes in western Ireland ([Irish Examiner, 2022](#)); and iv) pluvial flooding such as in June 2023 in parts of Kerry and Dublin ([Irish Times, 2023b](#)). In this report, the flooding in Midleton is investigated using a multi-step approach. In section 2, forensic analysis is presented that shows that extreme rainfall over multiple time scales was the primary driver of the event. In section 3, this extreme rainfall is assessed for its links to climate change using a multi-method multi-model attribution. In section 4, the results are combined with other lines of evidence describing physical drivers of changing risks of flooding in Midleton, and finally in section 5 the implications of the study across both science and risk management are explored.

² There was a [prior project](#) funded by the Irish EPA looking at extreme weather attribution and that did look at one case study finding, using their tools and techniques, no human influence.

2. Assessing drivers of Midleton flooding

In this section we systematically assess various possible contributory factors to the flooding in Midleton to alight on the final set of diagnostics to consider in Section 3 for the formal attribution study. This makes use of a broad range of measurements (principally from sites in Figure 4) as well as gridded products and various types of modelling.

2.1 The potential role of the ocean

The potential role of the ocean in Midleton flooding is well recognised in the Midleton Flood Relief scheme [documentation](#). Midleton is located at the confluence of the Owenacurra and Roxborough/Dungourney rivers near to their entry into the northeast of Cork Harbour. Tidal flooding can occur when naturally large astronomical factors combine with background factors such as sea level rise. The Cork region has seen almost double the amount of relative sea level rise of the Irish east coast, such as Dublin ([Pugh et al., 2021](#)). However, as noted, the flood event on the 18th October 2023 in Midleton luckily occurred at low spring tide (Figure 3 and associated discussion).

Elevated marine levels due to storm surge can also be ruled out as a contributory factor. Analysis of the Ringaskiddy tide gauge on the west of Cork Harbour shows no significant non-tidal residual (Figure 7). The sharp peak in the Bailick Road non-tidal residuals is associated with the strong outflow from the Owenacurra and Roxborough/Dungourney rivers following the flood event. Were the event to have been contributed to by a storm surge the signal would have been expected at both the Bailick road and Ringaskiddy gauges.

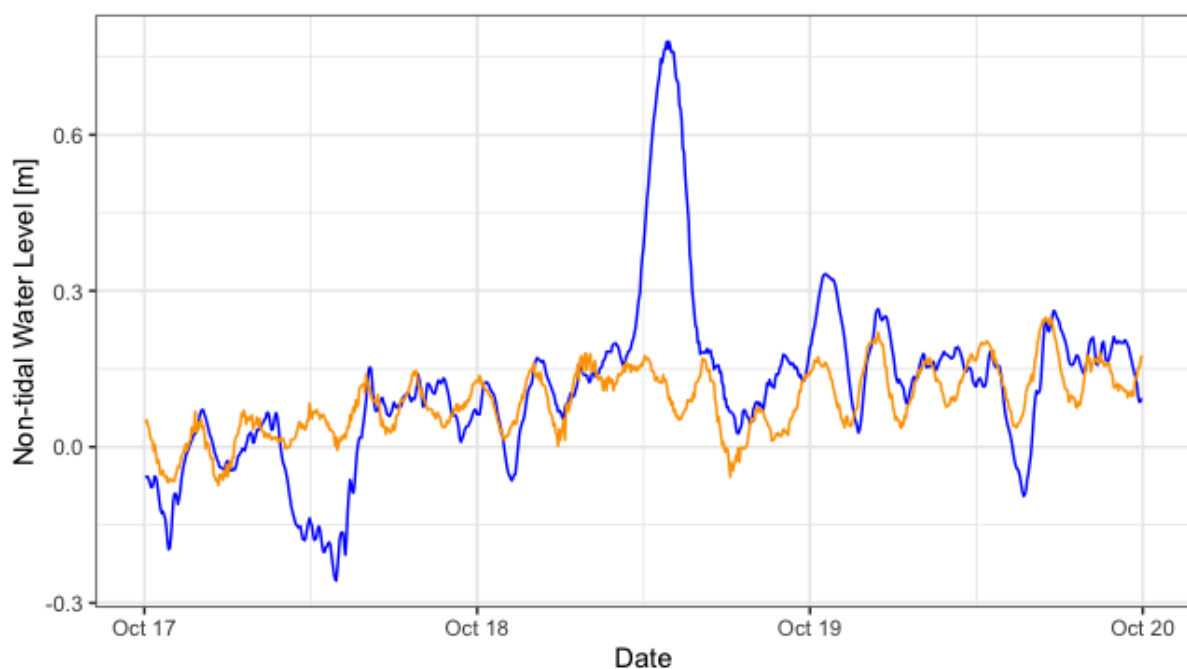


Figure 7: Non-tidal residuals over October 17th to 20th 2023 at Bailick Road (blue), near Midleton, and Ringaskiddy (orange), on the west side of Cork Harbour. See Figure 4 for locations of the two gauges.

Based upon the analysis of tidal gauge data, on this occasion not only was there no contribution arising from tidal locking or storm surge but the spring low tide actively helped to mitigate the impacts of the fluvial flooding by facilitating the fast release of the floodwaters into Cork Harbour and out into the Atlantic Ocean. Ocean factors are therefore not relevant in a formal attribution sense but were key in avoiding what could have been an even worse outcome for Midleton.

2.2 Evidence of fluvial flooding

The EPA provides water level and flow data for the Owenacurra catchment at Ballyedmond (gauge 19020), some 2.8 km upstream of Midleton. The observed daily record commences 15th June 1977, with 15-minute data available since 2000. The gauge is located at a natural channel cross section, with no structure (such as a weir) present. The control is therefore unstable and the rating curve used to relate water levels to flows is subject to change. As a result of this instability the gauge zero has been changed historically, as has the associated flow rating curve, with ten different rating curves in operation over the period of record, seven before 1995. However, a good sample of spot flow measurements have been made across low and high flows for rating curve development. It is notable however, that the Ballyedmond gauge does not appear among the 137 highest quality records for assessing high flows in Ireland compiled by the Office of Public Works (OPW) in developing their Flood Estimation Methodologies for Ireland (FEMI) dataset. The Storm Babet event constitutes the highest recorded river height value in the past 23 years (Figure 8) captured by the river gauge.

Water level (Ballyedmond)

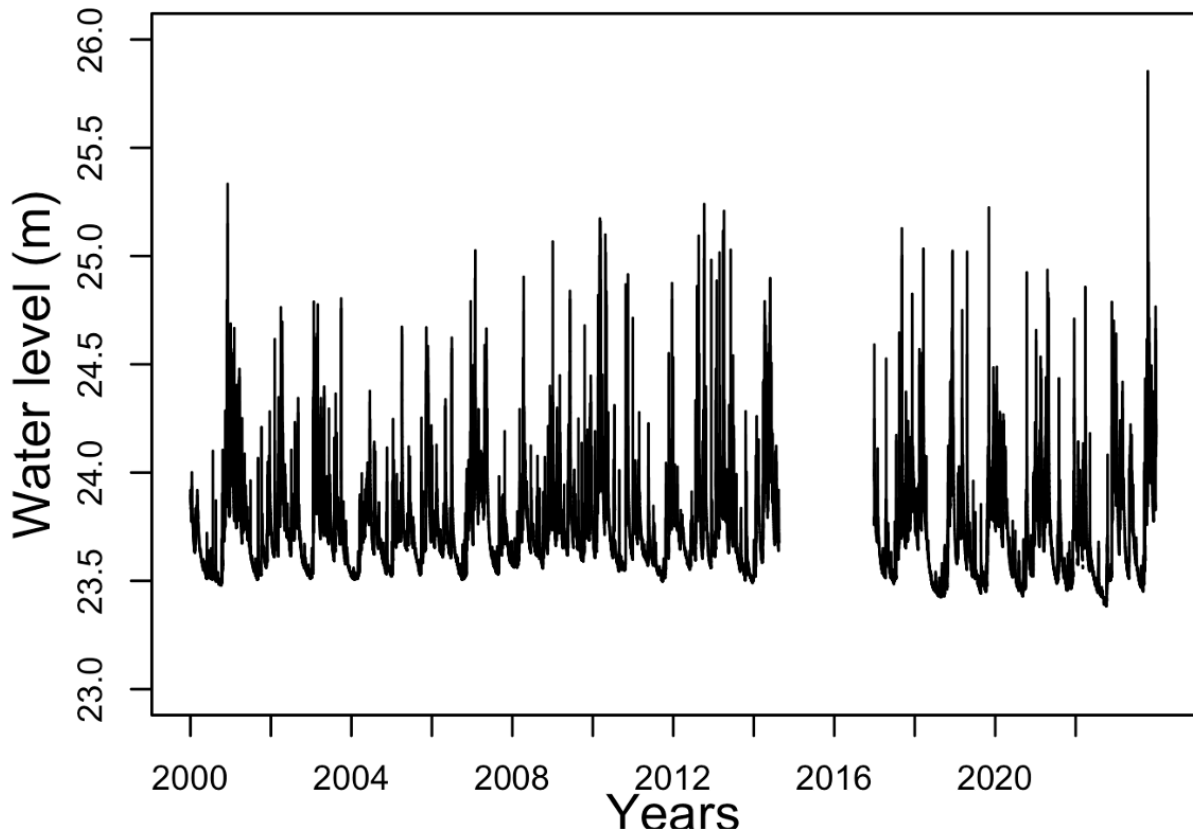


Figure 8: Water levels in the Owenacurra river at Ballyedmond (Midleton) from 2000-2023. Note that the series extends further back in time but not as a continuous 15-minute resolution series. Further note the gap over 2014-2016 which may miss important events of comparable or larger amplitude than that observed in 2023.

Figure 9 displays the ten highest peaks observed at the Ballyedmond gauge between 2000 and 2023 and their time evolution. As is typical for a small catchment such as the Owenacurra (78 km²) the discharge peaks are very fast (or 'flashy') with recession of the flood peak also rapid. The peak discharge lasts for a matter of a few hours before receding. This is consistent with reports of the flood event at Midleton which lasted a matter of hours. Despite the proximity to Cork Harbour there is little sign of tidal lock impacts across different flood events (see Section 2.1). Given that the river drops a further 24 metres in the matter of 3-4 Km to reach the Bailick Road tidal gauge this is perhaps unsurprising. To see the impacts of tidal lock would require a gauge much closer to or even in Midleton.

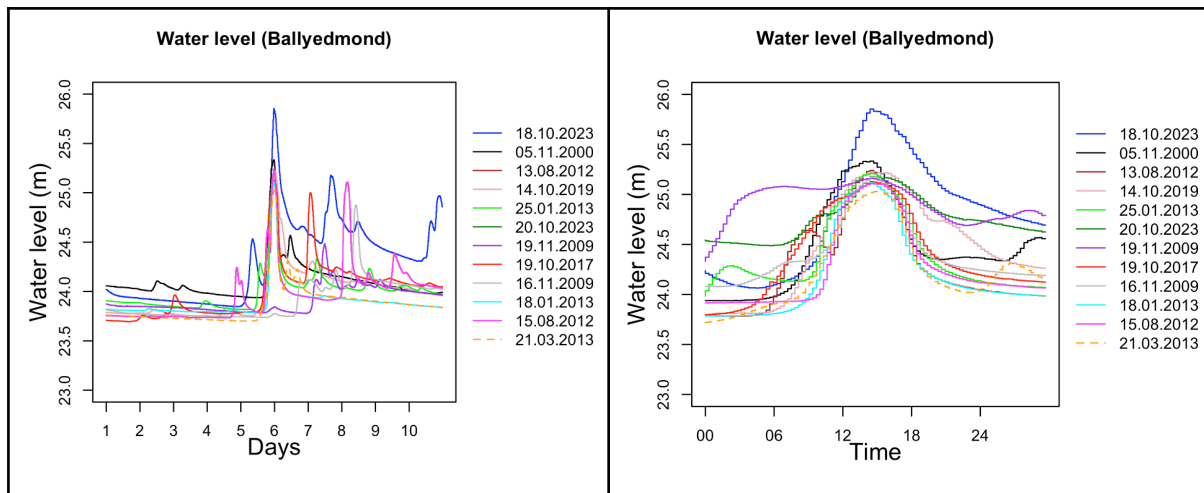


Figure 9: Water levels at Ballyedmond for the days (left) and hours (right) preceding and following each of the ten highest water levels recorded since 2000. Note that in the left hand plot the event on 20th October 2023 is omitted given that it is also present as $t+2$ days peak in the 18th October 2023 plot.

It is clear from the analysis of the EPA gauge and the analysis of Arup (2023^{a,b}) which documents the flooding event evolving from the upstream end of Middleton to the downstream reaches and makes frequent allusions to river based water ingress that the principal cause of the event relates to fluvial flooding. On the Owenacurra river at Ballyedmond the event was the most extreme water level recorded since 2000 when 15-minute resolution reporting became available (although note important gaps in the record and caveats around gauge quality). The next step is therefore to understand why this fluvial flood was so extreme.

2.3 Soil Moisture Deficit (SMD)

The Soil Moisture Deficit (SMD) is the amount of rainfall necessary to bring the moisture in the soil up to the total amount of water the soil can hold, known as the field capacity. When the soil is dry the SMD is positive, when the SMD is -10mm the soil is saturated. When rain falls on saturated soil, water is likely to pool and runoff as the soil cannot absorb any more water.

The SMD at a location on a particular day is given by the SMD on the previous day, the water lost from the soil due to drainage and actual evapotranspiration, minus the rainfall:

$$SMD_t = SMD_{t-1} - \text{Rainfall} + ET_a + \text{Drain} \quad (1)$$

The actual evapotranspiration, ET_a , is the water lost from the soil to the atmosphere due to vegetation and is closely related to the potential evapotranspiration but takes the amount of moisture in the soil into account – when the soil is dry the amount of water lost by the soil due to evapotranspiration will be less than what the vegetation can potentially transpire.

The actual SMD calculation is made by Met Éireann at synoptic stations where the necessary weather parameters are recorded and has three outputs relating to different soil drainage types: well drained, moderately drained and poorly drained soils. For this analysis, a moderately drained soil scenario is

used – there are water surpluses on wet days, but on dry days the drainage rate can be in excess of 10mm/day.

Daily SMD data is available from Roches Point from September 2014 to October 2023. A plot of the average daily values for the 8 years from 2015 to 2022 shows on average a positive SMD from March until October with the soil being at capacity or negative (SMD ≤ 0) from October to February (Figure 10). There is however a lot of variation in the SMD across the year, particularly when the SMD is positive, with this being driven by a variation in rainfall amounts and the drying effects of higher temperatures which result in higher evapotranspiration. Lower SMDs from October to February coincide with higher rainfall amounts and lower temperatures which lead to lower evapotranspiration.

Plotting SMD values for 2023 on the 2015-2022 daily distribution shows some deviation from typical values (Figure 10), though it is noted that 8 years of baseline SMD data is relatively short. There are periods in February-March and late May-early June where the SMD indicates the soil is drier than expected. Soil is wetter than expected at other times particularly from July to October.

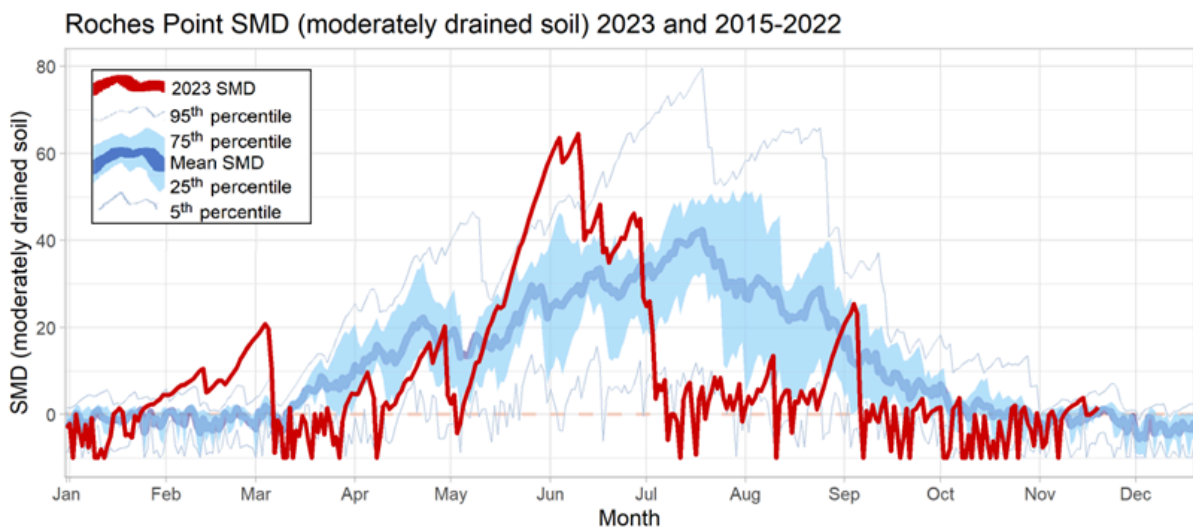


Figure 10: Calculated SMD at Roches Point, 14 Km south of Middleton, for a moderately drained soil by day of the year. Shown here is the average 2015-2022 (heavy blue line), with the 5th, 25th, 75th and 95th percentiles to highlight the variation in this parameter. Superposed are calculated SMD values for 2023 at Roches Point for a moderately drained soil by day of the year (red line).

The daily rainfall totals shown in Figure 11 help explain the variation in SMD. Higher SMDs coincide with extended dry spells while low SMDs are associated with extended sequences of rainfall. There are two days with peaks in rainfall above 50mm at Roches Point in 2023, August 18th (storm Betty) when 57.5 mm was recorded and on the 17th of October (storm Babet), when 73 mm of rainfall fell. Both show saturated soils at Roches Point, but for the October event, according to the SMD, the period of soil saturation extends until the 20th of October, a period of four days.

Roches Point SMD (moderately drained soil) 2023 and 2015-2022

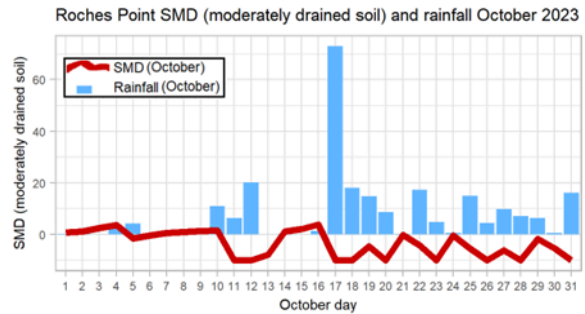
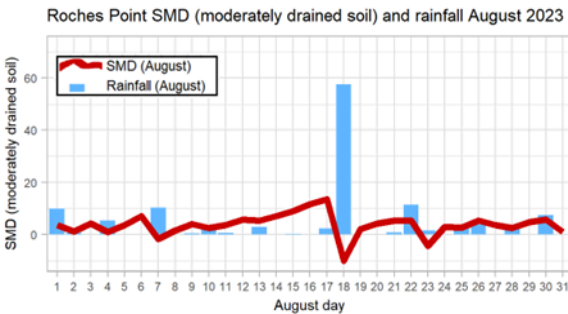
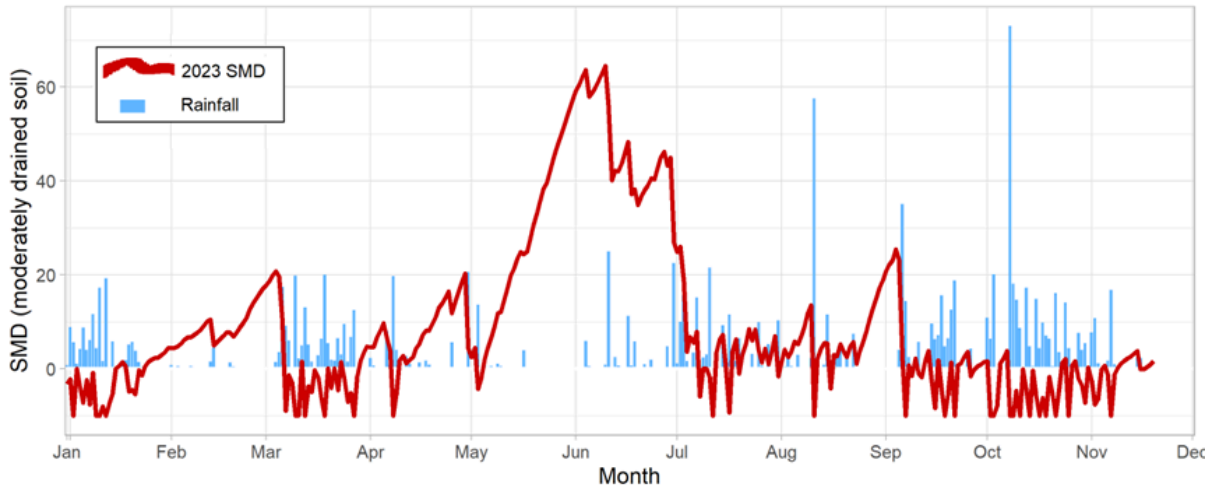


Figure 11: Top: 2023 daily SMD and rainfall recorded at Roches Point (red) alongside daily rainfall amounts (blue). Bottom: SMD and rainfall for August 2023 on the left and October 2023 on the right with the peak in rainfall in August associated with storm Betty and the October peak associated with storm Babet.

Interpreting the SMD at Roches Point as being a good proxy for conditions in the region during the October flooding event, the very high amount of rain falling on the 17th of October resulted in soils becoming quickly saturated. Excess rainfall not absorbed by the soil accumulates on the surface or runs off, thus contributing to the flooding experienced in the town.

2.4 Precipitation

2.4.1 Precipitation accumulations over preceding months

The period starting from July 2023 through to October 2023 was record wet across a number of datasets (Figure 12). As noted in Section 2.3 this pre-conditioned the catchment by saturating the soils over an extended period. Indeed, Figure 13 highlights via the Standardised Precipitation Index that the past 2 years and all sub-periods within the past year considered had been overall anomalously wet for the region as well as much of the country as a whole. The Standardised Precipitation Index ([McKee et al., 1993](#)) is calculated using gridded monthly rainfall data that is aggregated to catchment averages for each river catchment in the country.

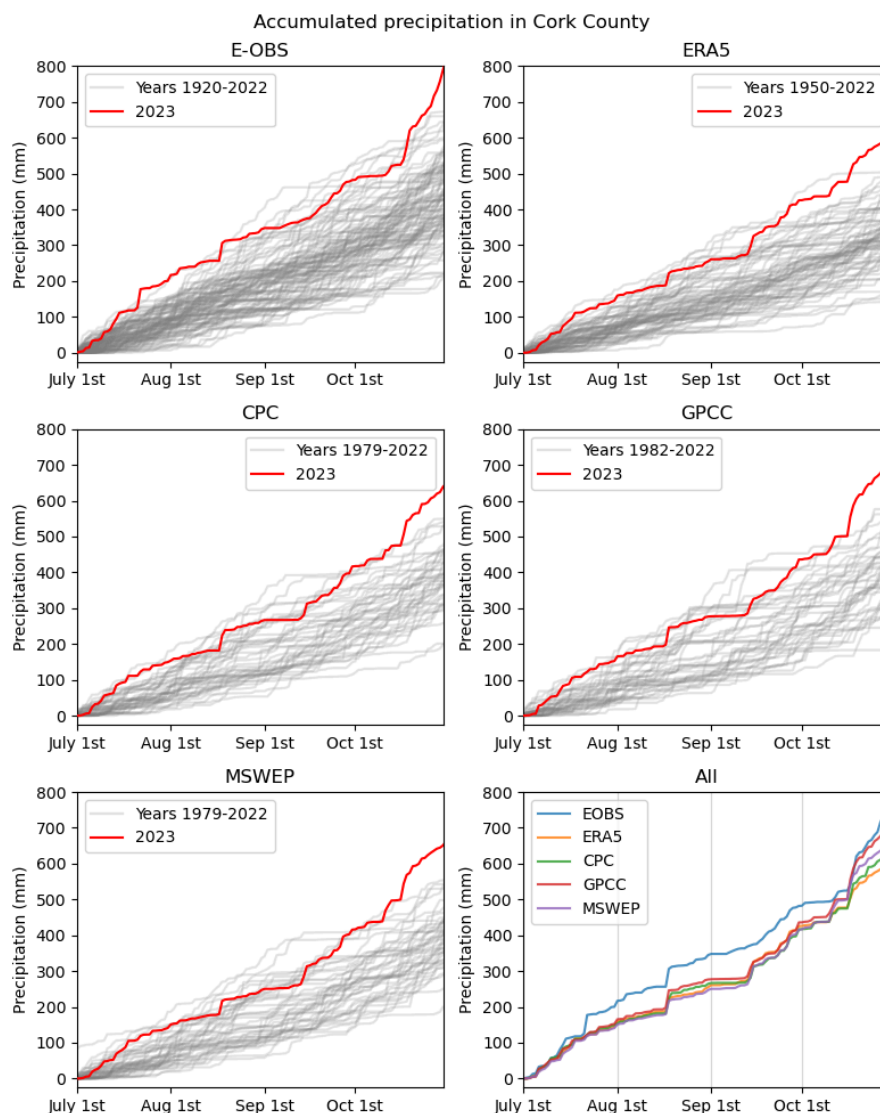


Figure 12: Cumulative precipitation estimates for County Cork from July 1st to October 31st averaged across the county from a range of observationally based estimates used in Section 3. In all cases 2023 represented a record cumulative precipitation for this 4 month period (note that periods of record differ). The final panel compares all the observationally based estimates together. These data are further discussed in Section 3.

Standardized Precipitation Index Values: October 2023**

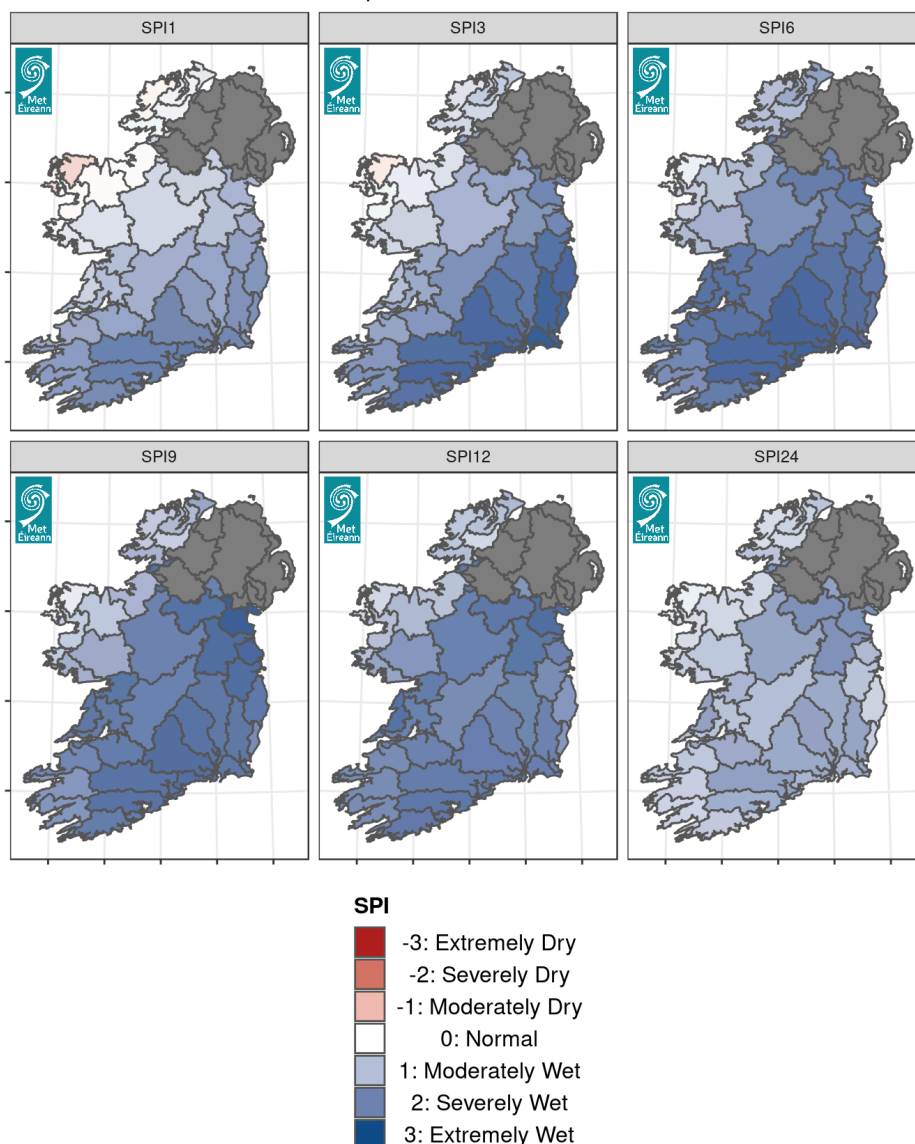


Figure 13: A map of the Standardised Precipitation Index (SPI) for the different time scales provides a spatial view of the situation for October 2023, from SPI1 (top left) to SPI24 (bottom right). Sourced from Met Éireann. In the Lee, Cork Harbour and Youghal Bay catchment area where Midleton is located, all SPI indices out to SPI24 had positive values at the end of October 2023 indicating above average precipitation across all timescales.

2.4.2 Precipitation accumulations over Storm Babet

The two day precipitation event associated with Storm Babet was an extreme rainfall event associated with a very strong spatial gradient from south to north across County Cork (Figure 14). Areas in SE County Cork in and around Midleton received widely in excess of 100mm from the two day precipitation event. Whereas areas in the north of the county within <100km of the coast received less than 50mm of precipitation.

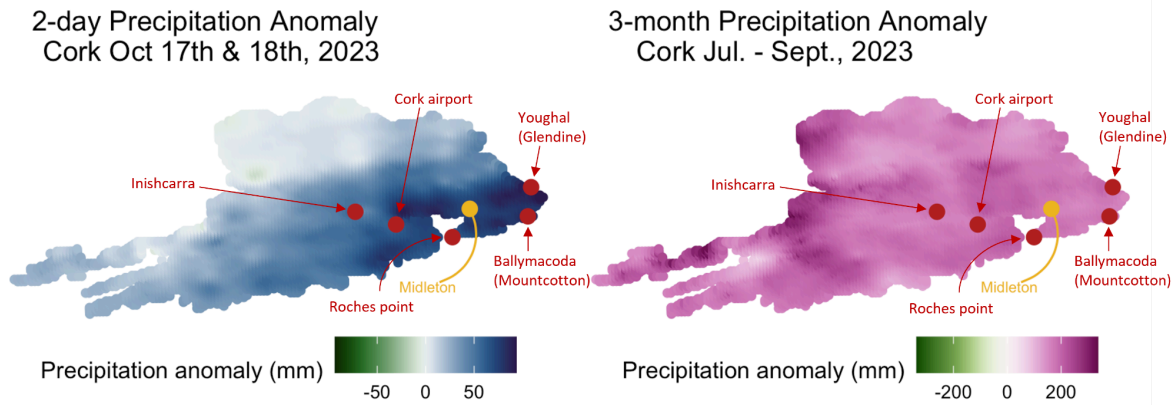


Figure 14: Rainfall anomalies for County Cork from the Met Éireann gridded product (see section 3.2.1 for details), showing the 2 days of Storm Babet (left) and July-September accumulations (right), each versus the 1980-2010 average for the same period and event type. In and around Midleton (SE County Cork) many areas received in excess of 100 mm of rainfall in two days due to Storm Babet, while the entire county received significantly above average rainfall for the preceding months.

Composite radar imagery from Met Éireann (Figure 15) shows the temporal evolution of the event over the island of Ireland. At the time Met Éireann were in the final commissioning phases of their new dual-polar radar system at Shannon airport and operational radar returns for SW Ireland were being undertaken from a temporary x-band radar installation some 8 kms north of Midleton. Unfortunately, the x-band radar suffers from attenuation issues in extreme precipitation events so accumulated totals are not reliable. Nevertheless, the 5 minute accumulations shown in Figure 15 provide robust indications of the temporal evolution of the event with several bands of organised precipitation crossing the region with embedded convection.

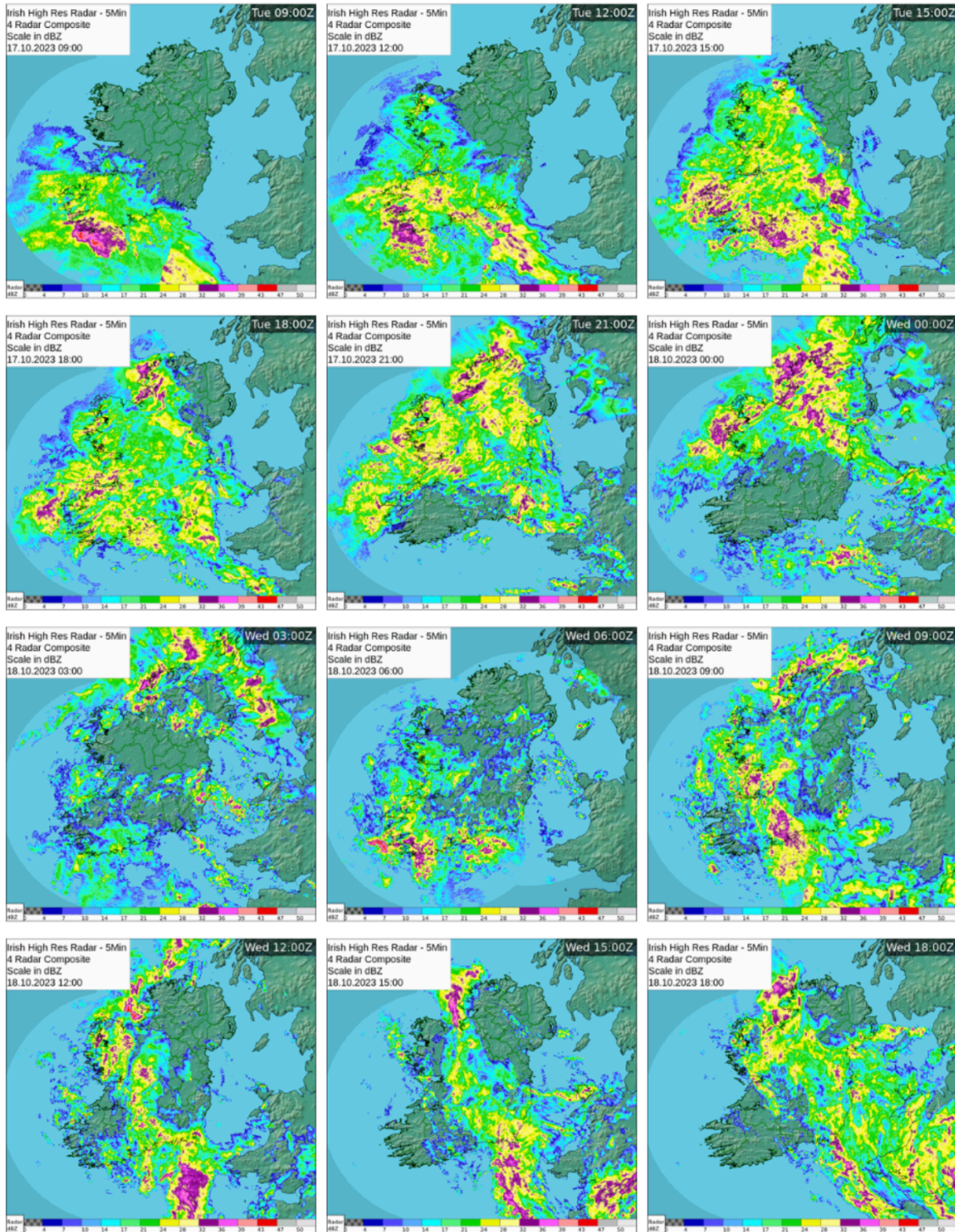


Figure 15: Met Éireann composite radar images for the period 09:00 on the 17th of October to 18:00 on the 18th October shown at 3-hour intervals.

The two day precipitation totals associated with Storm Babet averaged across County Cork were the most extreme October 2-day totals since at least the 1970s across a range of datasets (Figure 16).

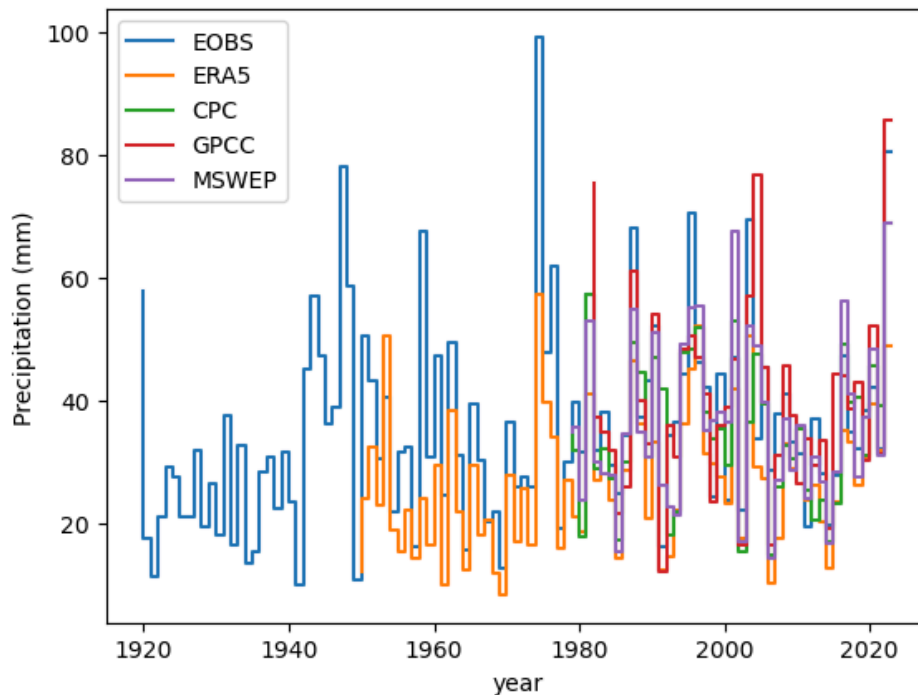


Figure 16: Two day October precipitation maxima across a range of datasets averaged over County Cork for October. The 2023 value is the Storm Babet event being analysed herein. Note that distinct datasets have distinct start dates. All values are actual values as reported in each product. These data are further discussed in Section 3.

2.5 Hydrological Analysis

2.5.1 Study Design, Data and Methods

Changes in river flows and floods can be driven by changes in climate but also by changes internal to the catchment, such as land use change that can modify rainfall runoff processes. Here we develop simulation models of October maximum flows in the Owenacurra catchment to investigate i) the most important rainfall variables driving maximum flows in October; ii) the role, if any, of landuse change in the catchment in modifying flood events, and; 3) given the relatively short flow record length at Ballyedmond, to extend/reconstruct the maximum October flow series back to 1941 using available meteorological data.

We employed two modelling approaches, namely a simple hydrological model and a statistical multiple regression approach. Given that both sets of models are driven by meteorological inputs only, we assume that their simulations represent climate driven changes in the October maximum flow series. To interrogate other plausible drivers of change internal to the catchment (e.g. landuse change or issues with data quality) we further interrogate the residuals (or differences) between the observed and simulated October maximum flow series for each model.

Analysis is based on the Owenacurra catchment at Ballyedmond (gauge 19020), located approximately 2.8 Km upstream of Midleton, draining a catchment area of approximately 78 Km². The gauge is located at a natural channel cross section and is noted as being unstable, with the rating curve at the site being subject to change over time. Observed daily discharge data for the period 16/6/1977 – 31/10/2023 were downloaded from the EPA Hydronet website.

The GR4J rainfall runoff model ([Perrin et al., 2003](#); [Coron et al., 2017](#)) was selected for use given its previous application in Ireland (e.g. [Meresa et al., 2022](#); [Donegan et al., 2021](#); [Golian and Murphy, 2021](#)) and its simple structure, requiring only four parameters to be calibrated. Catchment average precipitation was extracted from Met Éireann's gridded (1 X 1 Km resolution) daily dataset for the period concurrent with discharge observations. Daily Potential Evapotranspiration (PET) was derived using the method of [Oudin et al. \(2005\)](#) applied to daily catchment average temperature, extracted from Met Éireann's gridded (1 X 1 Km) temperature observations, also for the concurrent period. The GR4J model was calibrated for the period 1/1/2010 – 31/10/2023, validated over 1/1/1990-31/12/2009, before being used to simulate daily discharge from the catchment for the period 16/6/1977-31/10/2023. Model performance was largely insensitive to the period chosen for calibration. To calibrate the model 1000 parameter sets were sampled from a uniform distribution representing plausible ranges for each of the four model parameters. Simulations of daily mean flow from each parameter set were evaluated using the Nash- Sutcliffe (NS) objective function, with only those parameter sets returning an NS score > 0.70 being retained. Retained parameter sets were then evaluated during the testing period before being used to simulate October daily maximum flows for the entire series. Results are presented using a median simulation from across all retained parameter sets, together with 95 percent confidence intervals.

We also developed regression models of October maximum flows. A large number of plausible predictors were compiled comprising monthly and multi-month precipitation totals, maximum single and consecutive day (i.e. 1, 2, 5, 10, 20, 30, 50) precipitation totals, together with monthly and seasonal indices of key modes of climate variability, including the North Atlantic Oscillation and the East Atlantic Pattern. Exhaustive regression using the leaps package in R ([Lumley, 2020](#)) was used to identify predictors with additional testing of conditions that the selected predictors must be significant at the 0.05 level, while potential multicollinearity was tested by calculating the Variable Inflation Factor (VIF) score. Model performance was measured using R² as a measure of the amount of variance in the observations explained by the model. Selected models were used to simulate October maximum flows with model residuals further examined.

To assess residuals from each model of October maximum flows, we used the [Hilda+ landuse change dataset](#) ([Winkler et al., 2021](#)), as national or local land use change time series are not readily available. Hilda+ is a global 1Km X 1Km dataset of land use change over the period 1960-2019 derived from multiple, openly available land use change products. Full details on the generation of the Hilda+ dataset are provided by [Winkler et al. \(2021\)](#). The dataset provides estimates of land use change across six generic land cover categories (Urban areas, Cropland, Pasture/rangeland, Forest, Unmanaged grass/shrubland and sparse or no vegetation). Due to uncertainties in the classification between types of grassland, we combined Pasture/rangeland and Unmanaged grass/shrubland into a single 'Grassland' category. The Hilda+ data for the Owenacurra catchment were extracted and used to compile a time series of percent cover estimates of Grassland, Forest and Cropland for the catchment for each year, concurrent with model residuals. To extend these data to 2023, the percent cover for each category in 2019 (i.e. the end of the Hilda+ dataset) was used to represent each

subsequent year. These data, together with time (Year) were used as predictors and regressed onto model residuals to examine if i) there is evidence of increasing/decreasing residuals over time, not captured by the model, and ii) if available land use change data can explain any pattern in the model residuals. All possible predictors (Year, Grassland, Forest, Cropland) were evaluated for significance at the 0.05 level and model performance evaluated using R^2 (the percentage of explained variance).

2.5.2 Results

The GR4J model performed well in simulating daily mean flows for the Owenacurra catchment with 1000 parameter sets retained for simulation returning NS scores of 0.83 - 0.91 in calibration and 0.72 - 0.91 in validation. In addition to GR4J, two regression models of October maximum flows were selected. Both are simple two variable models with the first predictor in each being the maximum 2 day rainfall in October. The second predictor represents antecedent conditions, with model 1 using July, August and September (JAS) total precipitation, while model 2 employs cumulative totals for August, September and October (ASO). Both models are statistically significant (0.05 level), return good R^2 scores (Model 1: 0.78; Model 2: 0.82), with all predictors being significant at the 0.05 level and no issues of multicollinearity evident.

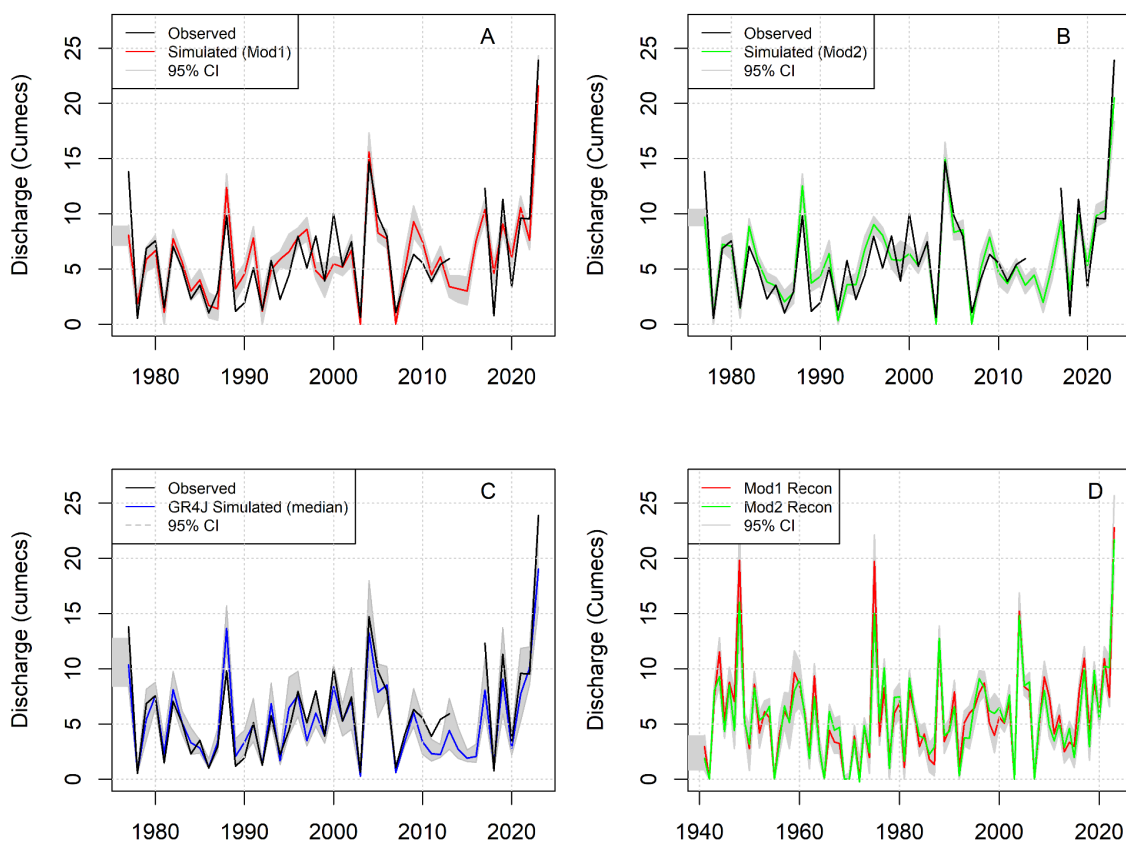


Figure 17: Observed and simulated October maximum flows for the period 1977-2023 both regression models (A and B) and the GR4J hydrological model (C), together with reconstructions of the October maximum flow series to 1941 using both regression models (D). In each plot the shaded grey area

represents the 95 percent confidence intervals of model simulations. Colours for each data type are identical between panels for ease of interpretation. See inline keys.

Figure 17 shows the observed and simulated October maximum flow series for each regression model (Fig 17.A and 17.B) and for GR4J (Fig. 17.C). All three models perform well across the series, and indicate the exceptional nature of the October 2023 maximum in the context of the available record. Each model does underestimate the magnitude of the 2023 peak, with the regression models doing better than the GR4J model. This underestimation may be due to data errors, for example an underestimation of catchment precipitation, and/or other drivers of change internal to the catchment, such as land use change (see next paragraph). Both regression models were also used to reconstruct the October maximum flow series back to 1941 (Figure 17. D) to contextualise the magnitude of the 2023 flood. The reconstructions indicate that 2023 was the largest October maximum flow in at least the last ~80 years, including for the missing years of flow observations from 2014-2016.

To investigate if other drivers, besides climate, may be associated with an increase in October maximum flows, we analysed model residuals for GR4J, model 1, model 2 and the median residual across all three models, as indicated above. The time series of residuals for each model is shown in Figure 18.A. First, the variable 'Year' was used as a predictor to examine if there is any monotonic increase or decrease in residuals over time. For model 1 and the median simulation across all three models, no evidence of change over time in the residuals was found. For GR4J and model 2 Year returned a p-value of 0.06 and 0.04, respectively, with residuals increasing over time. Second, for GR4J and model 2 we used available land use change data as a predictor to examine if one or more categories of land use change were a significant predictor of model residuals. Figure 18.B shows available land use change data from Hilda+ for the Owenacurra catchment, which indicates a decrease in grassland and an increase in forest cover over time. Change in forest cover was found to be a marginally significant predictor of residuals for both GR4J ($p = 0.05$) and model 2 residuals ($p = 0.06$), with Year no longer a significant predictor after the inclusion of forest change. However, for both models a relatively small proportion of the variance in model residuals was found to be explained by forest change, with an R^2 of 0.25 returned for GR4J and 0.08 for model 2. Therefore, while change in forest cover may be a significant predictor of residuals for GR4J and model 2, it has a relatively minor role in explaining change in October maximum flows. Moreover, model 1 and the median simulation across models show no evidence of changing residuals over time nor of any land use change influencing model residuals. We also note the uncertainty associated with the Hilda+ land use dataset.

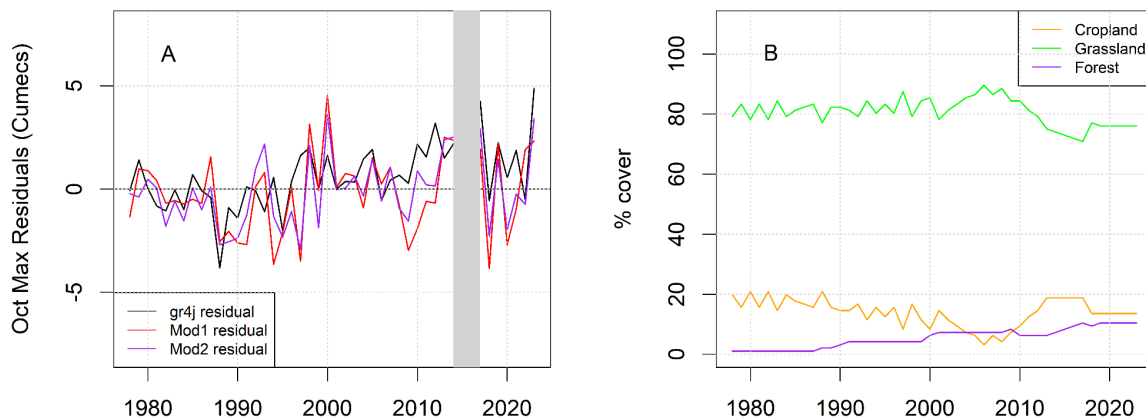


Figure 18: Residuals (difference between observed and simulated October maximum flows) for each of the three models developed (A), together with estimates of percent cover for different land use categories in the Owenacurra catchment for the period 1977 -2023 derived from the Hilda+ dataset (B). The vertical shaded area in A represents a period of missing data in the observations.

2.5.3 Conclusion

The hydrological analysis undertaken shows that simple models can successfully reconstruct October maximum flows in the Owenacurra catchment. Each of the three models developed show the extreme nature of the October 2023 flood event, which stands out as the largest flood event in the available observational record (back to 1977), and even over at least the last ~80 years when October maximum flows are reconstructed back to 1941. The regression models developed show that maximum two day precipitation in October and antecedent precipitation (represented by the previous three month precipitation totals) are good predictors of October maximum flows in the catchment. These variables are therefore a sensible choice for further investigation of an anthropogenic climate change signal in the meteorological drivers of the October 2023 flood event. Moreover, the analysis shows that precipitation is the main driver of change in October maximum flows over time. Analysis of model residuals shows that while land use change, in the form of an increase in forest cover, can explain a small proportion of the variance in the residuals from two of the three models developed, the effect is on the whole relatively minor, especially for the regression models. Additional sources of error in model simulations relate to well known observational challenges, including the difficulties in capturing true rainfall totals across the catchment and uncertainties in estimating flows given the extreme nature of floods and the unstable control at the Ballyedmond gauge.

3 Attribution of extreme rainfall to anthropogenic climate change

3.1 Event definition

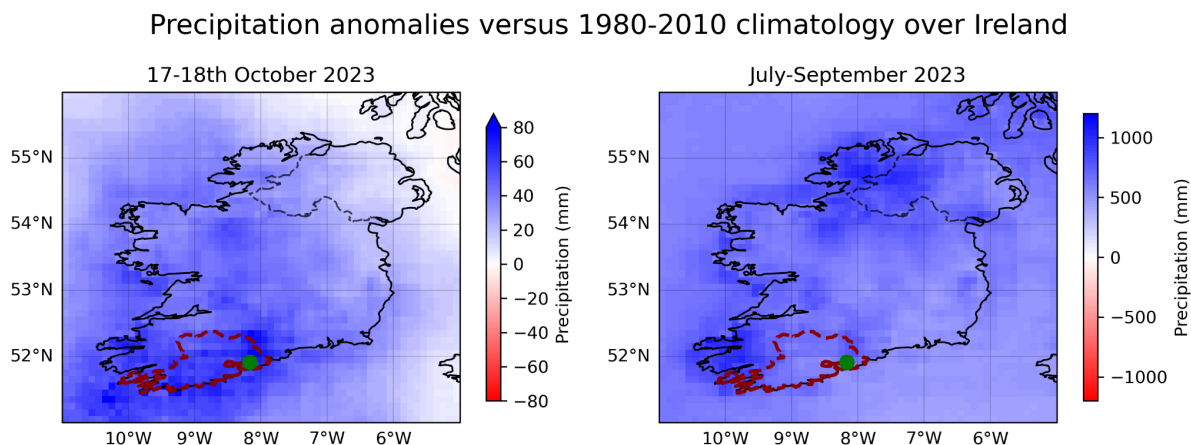


Figure 19: Rainfall anomalies for Midleton (green dot) County Cork (red) and Ireland from MSWEP, showing the 2 days of Storm Babet (left) and July-September accumulations (right), each versus the 1980-2010 average for the same period.

Section 2 of this report presented forensic analysis that showed that the flooding in Midleton on October 18th 2023 was largely driven by the occurrence of extreme rainfall. Specifically, it was characterised by short pulses of rainfall associated with Storm Babet over the course of ~2 days, falling on top of soils saturated by above-average rains since July, leading to exceptional flow rates. Therefore, in order to assess the contribution of anthropogenic climate change to the flooding, we consider changes in both maximum 2-day accumulated rainfall in October, and total accumulated rainfall from July-September (Figure 14, Figure 19).

The rainfall totals are assessed over the entirety of County Cork, rather than only the relatively small catchments that led to the flooding in Midleton, for several reasons. First, much of southwestern Ireland is subject to a similar climate and experienced similar extremes that led to the flooding in 2023. Thus, to balance the local scale of this flooding with achieving a broader applicability to risks in Ireland, the county provided an ideal spatial scale that is also physically and societally relevant as an administrative region at which risks may be addressed. Second, this spatial scale enables the use of reanalysis and climate models that are often relatively coarse in resolution and could not accurately capture the shape of the river catchments upstream of Midleton.

Overall, the event is characterised as the maximum of 2-day accumulated October precipitation, and the total July-September accumulated precipitation, both averaged over County Cork. This means that the results are applicable to County Cork, and to a lesser degree large parts of southern and western Ireland.

3.2 Data and methods

3.2.1 Observational data

Rainfall observations from individual stations were obtained from the National Climate Archive at Met Éireann. Rainfall is recorded at climate and synoptic stations and through a network of voluntary rainfall observers. At climate and voluntary rainfall stations, a daily rainfall total is recorded each day at 0900 UTC, and the total is assigned to the previous day. At synoptic stations, rainfall readings are continuously reported on the hour. The study looked at daily rainfall data from 76 stations around the Middleton area. Only the 5 stations that had more than 47 years of data were included in the study. The longest running station is Roches Point which has a 140-year continuous record of daily rainfall observations from 1883 – 2023. Daily rainfall totals were summed to provide the 2-day accumulated rainfall total for the period 17-18th October and the 3-month accumulated rainfall total for the period July to September 2023.

Several gridded observational and reanalysis products were also used to explore this event:

- Met Éireann's 1 km x 1 km gridded rainfall dataset (approximately $0.01^\circ \times 0.01^\circ$), derived from station-based observations for the period 1941-2023 were used to extract average rainfall values for the Cork region. The number of stations used to generate the gridded data available varies from year to year, but currently consists of approximately 500 stations over Ireland. Further information on the preparation of these datasets can be found in ([Walsh et al., 2012](#)).
- E-OBS (version 28.0e), is a $0.25^\circ \times 0.25^\circ$ gridded temperature dataset of Europe, formed from the interpolation of station-derived meteorological observations ([Cornes et al., 2018](#)).
- The European Centre for Medium-Range Weather Forecasts, or the ERA5 reanalysis product begins in the year 1950 ([Hersbach et al., 2020](#)). We use precipitation data from this product at a spatial resolution of $0.5^\circ \times 0.5^\circ$. It should be noted that the variables from ERA5 are not directly assimilated, but these are generated by atmospheric components of the Integrated Forecast System (IFS) modelling system.
- The Multi-Source Weighted-Ensemble Precipitation (MSWEP) datasets v2.8 (updated from [Beck et al., 2019](#)) combine gauge-, satellite-, and reanalysis-based data for reliable precipitation estimates, at 3-hourly intervals from 1979 to near real-time, and at 0.1° spatial resolution globally.
- GPCC Full Data Daily Product Version 2022 of daily global land-surface precipitation totals based on precipitation data provided by national meteorological and hydrological services, regional and global data collections as well as WMO GTS-data ([Ziese et al., 2022](#)). It is provided at a regular latitude/longitude grid with a spatial resolution of $1.0^\circ \times 1.0^\circ$ and covers the time period from January 1982 to November 2023. Relative precipitation anomalies at the stations (daily totals divided by monthly total) are interpolated by means of a modified SPHEREMAP scheme ([Becker et al., 2013](#); [Schamm et al., 2014](#); [Schneider et al., 2018](#)) and then superimposed on the GPCC Full Data Monthly Version 2022 ([Schneider et al., 2022](#)) monthly precipitation totals with climatological infilling. This is used only as a reference

dataset for investigation of the event due to the availability of other gridded data products for the region at a higher resolution and/or over a longer period.

- The CPC Global Unified Gauge-Based Analysis of Daily Precipitation data, that is provided by the NOAA PSL, Boulder, Colorado, USA, from their [website](#). This data is available at $0.5^\circ \times 0.5^\circ$ resolution, for the period 1979-present. This is used only as a reference dataset for investigation of the event due to the availability of other gridded data products for the region at a higher resolution and/or over a longer period.

Finally, as a measure of anthropogenic climate change we use the (low-pass filtered) global mean surface temperature (GMST), where GMST is taken from the National Aeronautics and Space Administration (NASA) Goddard Institute for Space Science (GISS) surface temperature analysis (GISTEMP, [Hansen et al., 2010](#) and [Lenssen et al. 2019](#)).

3.1.2 Model and experiment descriptions

To analyse the influence of GMST on the extreme rainfall contributing to the event, we use 2 multi-model ensembles from climate modelling experiments using very different framings ([Philip et al., 2020](#)): Regional climate models and sea surface temperature (SST) driven global circulation high resolution models, described as follows:

1. Coordinated Regional Climate Downscaling Experiment (CORDEX)- European Domain (EURO-CORDEX) with 0.11° resolution (WAS-22) ([Jacob et al., 2014](#); [Vautard et al., 2021](#)). The ensemble used here consists of a subset of 8 regional climate models each of which are driven by 6 GCMs. These simulations are composed of historical simulations up to 2005, and extended to the year 2100 using the RCP8.5 scenario. The subset consists of only those simulations passing various quality checks (see 3.1.3.1).

2. HighResMIP SST-forced model ensemble ([Haarsma et al. 2016](#)), the simulations for which span from 1950 to 2050. The SST and sea ice forcings for the period 1950-2014 are obtained from the $0.25^\circ \times 0.25^\circ$ Hadley Centre Global Sea Ice and Sea Surface Temperature dataset that have undergone area-weighted regridding to match the climate model resolution (see Table B). For the ‘future’ time period (2015-2050), SST/sea-ice data are derived from RCP8.5 (CMIP5) data, and combined with greenhouse gas forcings from SSP5-8.5 (CMIP6) simulations (see Section 3.3 of Haarsma et al. 2016 for further details).

3.1.1.3 Statistical methods

In this analysis we analyse time series from County Cork of precipitation values where long records of observed data are available. Methods for observational and model analysis and for model evaluation and synthesis are used according to the World Weather Attribution Protocol, described in [Philip et al. \(2020\)](#), with supporting details found in van [Oldenborgh et al. \(2021\)](#), [Ciavarella et al. \(2021\)](#) and [here](#).

The analysis steps include: (i) trend calculation from observations; (ii) model validation; (iii) multi-method multi-model attribution and (iv) synthesis of the attribution statement. We calculate the return periods, Probability Ratio (PR; the factor-change in the event's probability) and change in intensity of the event under study in order to compare the climate of now and the climate of the past, defined respectively by the GMST values of now and of the preindustrial past (1850-1900, based on the [Global Warming Index](#)). To statistically model the extreme 2-day October accumulations, we use a generalised extreme value (GEV) distribution that scales with GMST, while for the 3 month accumulations from July-September we use a normal distribution that scales with GMST. Next, results from observations and models that pass the validation tests are synthesised into a single attribution statement.

3.1.2 Observational analysis: return period and trend

In this section trends in observational datasets are calculated and compared. This primarily involves the gridded data products set out in section 3.2.1, supplemented by analysis of individual weather stations based at Roches point, Cork airport, Youghal (Glendine), Ballymacoda (Mountcotton), and Inishcarra (Figure 14). The role of individual stations is to provide an additional layer of evidence for the crucial observational basis of the study. We do not expect these time series to give statistically significant trends due to local-scale variability, nor will they be the same as the gridded product values because they are averaged over the county scale. However, the direction of change and the observed magnitude of the event at proximate locations provide a sanity check on what we ought to expect from gridded products.

For each event definition, the results of trend fitting are presented in tables, with gridded products and individual stations separated (Tables 2-5). An illustration of the calculated trend and statistical fit are also displayed, using the E-OBS dataset as an example (Figures 20 & 21).

3.1.2.1 2-day October maximum accumulations

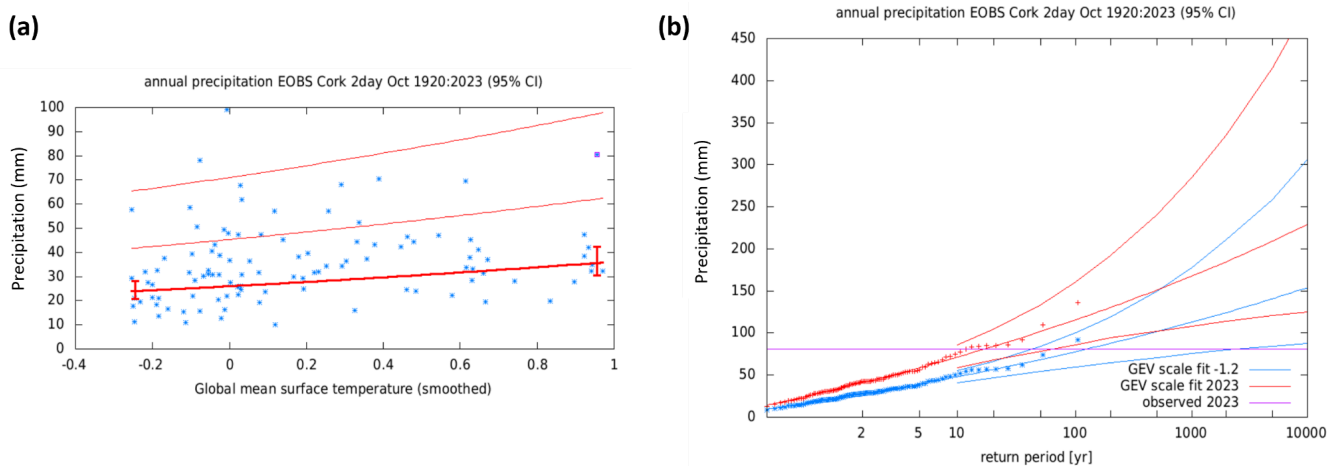


Figure 20: GEV fit to maximum 2-day October precipitation events over County Cork from 1920-2023 from the E OBS dataset. a) The observed distribution scaling with the covariate GMST and resultant trend. The 2023 event is highlighted in the purple box. b) Return periods of events if they occurred in

2023 (red) or in a 1.2 degree cooler world (blue). The 2023 event magnitude is highlighted by the purple line.

| Data | 2023 event magnitude (mm) | Return Period (2023) | Return Period (-1.2 C) | Probability Ratio | PR range (95% CI) |
|-----------------------------|---------------------------|----------------------|------------------------|-------------------|-------------------|
| ERA5 | 48.98 | 8.02 | 82.68 | 10.31 | 1.83 - 2156 |
| E-OBS | 80.46 | 16.38 | 120.14 | 7.33 | 2.20 - 96.08 |
| MSWEP | 68.85 | 32.15 | 300.17 | 9.34 | 0.29 - inf |
| Met Éireann gridded product | 66.91 | 12.76 | 29.95 | 2.35 | 0.30 - 24.34 |

Table 2: Results from trend analysis of 2-day October maximum rainfall for several gridded observational and reanalysis datasets. Statistically significant increases in probability are highlighted in dark blue, while non-significant increases are highlighted in light blue.

| Data | 2023 event magnitude (mm) | Return Period (2023) | Return Period (-1.2 C) | Probability Ratio | PR range (95% CI) |
|-------------------------|---------------------------|----------------------|------------------------|-------------------|-------------------|
| Roches point (1075) | 91.1 | 96.72 | 1115 | 11.53 | 1.24 - 1.5E06 |
| Cork Airport (3904) | 95.7 | 20.30 | 106.54 | 5.25 | 0.21 - 5056.7 |
| Youghal Glendine (4106) | 135.5 | 86.83 | 2065.6 | 23.79 | 1.91 - inf |
| Ballymacoda (4404) | 121.6 | 128.76 | 2307.3 | 17.92 | 0.40 - inf |
| Inishcarra (3704) | 95.3 | 74.33 | 132.63 | 1.78 | 0.50 - 224.95 |

Table 3: Results from trend analysis of 2-day October maximum rainfall for several stations around Midleton. Statistically significant increases in probability are highlighted in dark blue, while non-significant increases are highlighted in light blue.

3.1.2.2 July - September accumulations

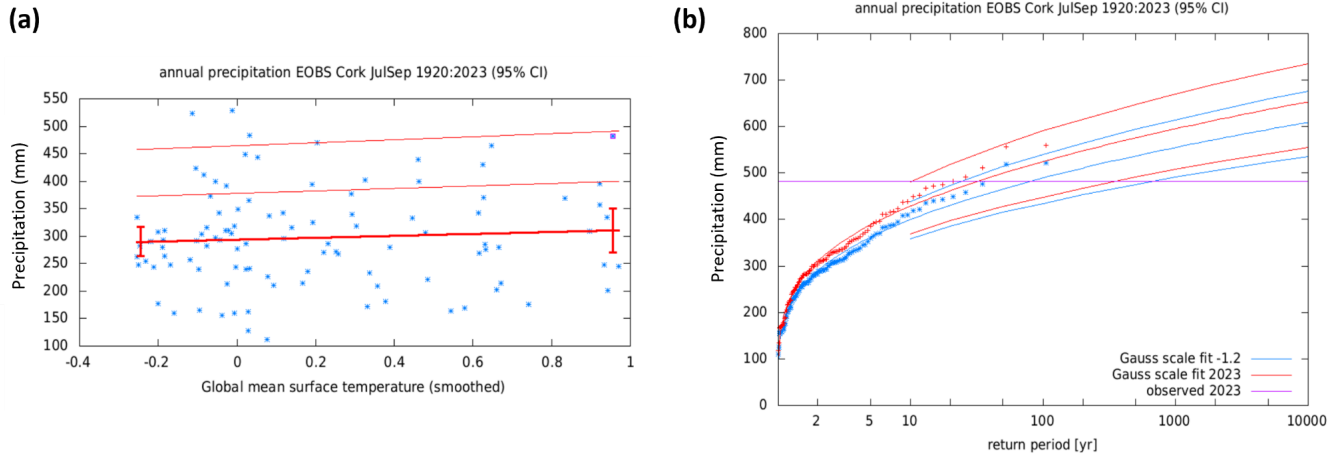


Figure 21: Gauss fit to July-September precipitation over County Cork from 1920-2023 from the EOBS dataset. a) The observed distribution scaling with the covariate GMST and resultant trend. The 2023 event is highlighted in the purple box. b) Return periods of events if they occurred in 2023 (red) or in a 1.2 degree cooler world (blue). The 2023 event magnitude is highlighted by the purple line.

| Data | 2023 event magnitude (mm) | Return Period (2023) | Return Period (-1.2 C) | Probability Ratio | PR range (95% CI) |
|-----------------------------|---------------------------|----------------------|------------------------|-------------------|-------------------|
| ERA5 | 425.53 | 67.92 | 321.43 | 4.73 | 0.42 - 1610 |
| E-OBS | 481.86 | 31.85 | 79.70 | 2.50 | 0.14 - 36.11 |
| MSWEP | 415.80 | 31.03 | 154.98 | 4.99 | 0.2 - 12600 |
| Met Éireann gridded product | 502.18 | 33.52 | 35.92 | 1.07 | 0.04 - 18.88 |

Table 4: Results from trend analysis of July - September rainfall for several gridded observational and reanalysis datasets. Non-significant increases in probability are highlighted in light blue. The overall return period was taken as 30 years.

| Data | 2023 event magnitude (mm) | Return Period (2023) | Return Period (-1.2 C) | Probability Ratio | PR range (95% CI) |
|--------------------------------|---------------------------|----------------------|------------------------|-------------------|-------------------|
| Roches point (1075) | 406.91 | 293.31 | 97.91 | 0.33 | 0.007 - 3.95 |
| Cork Airport (3904) | 434.90 | 31.42 | 224.34 | 7.14 | 0.096 - 535.57 |
| Youghal Glendine (4106) | 479.00 | 78.36 | 511.08 | 6.52 | 0.023 - 2724.2 |
| Ballymacoda (4404) | 414.80 | 64.16 | 291680 | 4546 | 0.13 - 3.1E10 |
| Inishcarra (3704) | 395.50 | 283.73 | 21.52 | 0.076 | 0.0001 - 5.01 |

Table 5: Results from trend analysis of July - September rainfall for several stations around Midleton. Non-significant increases in probability are highlighted in light blue, while non-significant decreases in probability are highlighted in light orange.

For 2-day October extreme precipitation, the stations give higher magnitude events than the gridded products (Tables 2 & 3). This is expected because the stations are clustered around Midleton, towards the east of the county, where the rainfall anomalies were greatest on the 17-18th October (Figure 14). Over the whole county, ERA5 records the lowest magnitude, while E-OBS gives the largest, but all are in reasonable agreement with the Met Éireann gridded product. The estimated return periods across these datasets vary between 8-32 years, so 20 years was taken as the best estimate for further analysis.

Changes in the likelihood of the observed extremes are also fairly consistent across datasets. ERA5 and E-OBS show statistically significant increases in likelihood while MSWEP and the Met Éireann dataset show non-significant increases. This is likely partly due to the shorter length of the MSWEP dataset, available from only 1979, while the Met Éireann dataset shows an overall weaker trend than remaining gridded products. Confidence is high in the observed increase because agreement is also strong between gridded and station data, with all showing best estimates of increasing likelihood. Notably, Roches Point, the longest station time series, shows a significant increase in likelihood despite earlier caveats around localised time series'.

For July-September accumulated precipitation, the stations give very similar magnitude events to the gridded products (Tables 4 & 5). Again this is expected because the anomalies around Midleton for this period were not significantly different to the wider county (Figure 14). The Met Éireann gridded product records the largest magnitude event with E-OBS showing the closest agreement. The estimated return periods across these datasets vary between 31-68 years, but 3 of the 4 estimates lie between 31-34 years, so 30 years was chosen for further analysis.

Changes in the likelihood of the observed event are also fairly consistent across datasets. No dataset shows a statistically significant increase in likelihood, but all gridded products and 3 of 5 stations give non-significant increases, with non-significant decreases for the other two stations. This suggests that the likely change is an increase but that any trend due to changes in GMST is highly uncertain, and as such has very low confidence.

3.1.3 Multi-method multi-model attribution

3.1.3.1 Model evaluation

In order to ensure that the climate models used to evaluate the changes in extremes are fit for purpose, a model evaluation procedure is carried out first. This involves 3 aspects of the observational data that the model should be able to reproduce:

1. Seasonal cycles - models must capture the seasonal cycle of precipitation in County Cork, with a focus on increases in autumn and winter and a decrease in summer.
2. Spatial patterns - models must capture the annual spatial pattern of precipitation over Ireland and the western UK.
3. Fit parameters - the statistical fit parameters must lie within the equivalent observational parameter uncertainty range (good), or their uncertainty ranges must overlap (reasonable)

Models are categorised as ‘good’ (if all evaluation metrics are ranked as good), ‘reasonable’ (if any are reasonable but none are bad), or ‘bad’ (if any aspects return bad). If an ensemble contains 5 or more good models, then only these are used. If not, then good and reasonable models are used. Bad models are always discarded. The figures and tables used for model evaluation are presented in the supplementary material (Figs. S2-5). From the CORDEX ensemble, 11 good models are used for the October precipitation and 8 for July-September. From HighResMIP, no models were good so 12 reasonable models were used for the October precipitation and 11 for July-September.

3.1.3.2 Results

This section shows Probability Ratios and change in intensity ΔI for models and also includes the values calculated from the fits with observations. For the event definitions described above we evaluate the influence of anthropogenic climate change on the events by calculating the probability ratio as well as the change in intensity using observations and climate models. Models which do not pass the validation tests described above are excluded from the analysis. The aim is to synthesise results from models that pass the evaluation along with the observations-based products, to give an overarching attribution statement. Figs. 21-24 show the changes in probability and intensity for the observations (blue) and models (red). To combine them into a synthesised assessment, we neglect common model uncertainties beyond the intermodel spread that is depicted by the model average, and compute the weighted average of models (dark red bar) and observations (dark blue bar): this is indicated by the magenta bar ([Philip et al., 2020](#); [Li & Otto, 2022](#)).

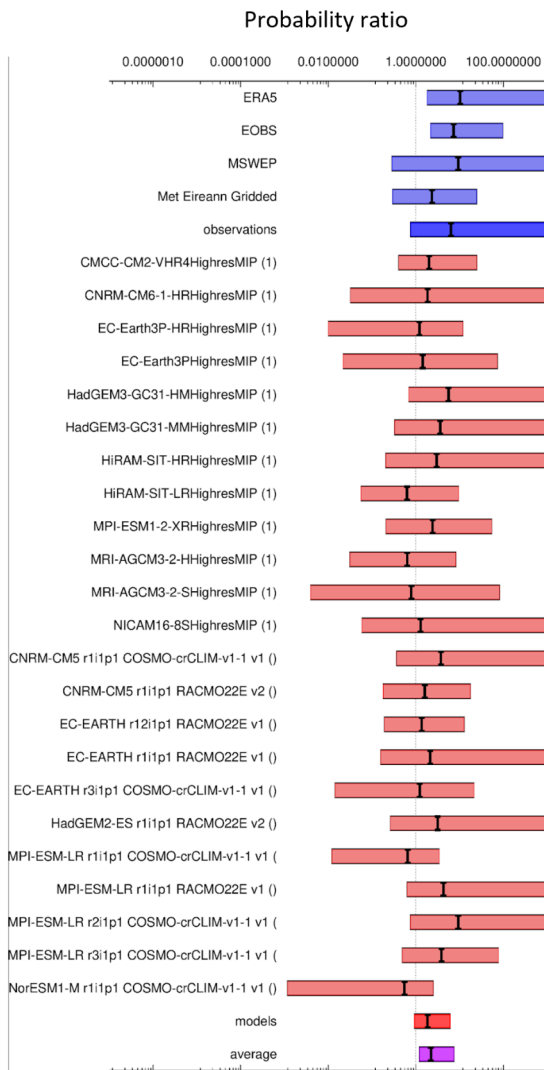
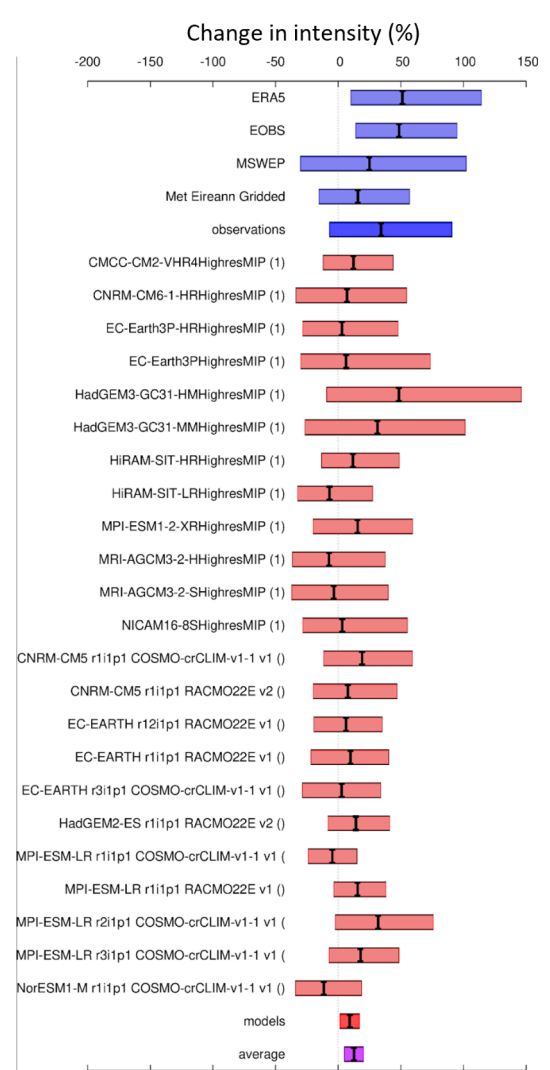
(a)**(b)**

Figure 22: Synthesis of (a) probability ratios and (b) intensity changes when comparing the 2-day maximum October precipitation that occurred in 2023 with a 1.2 degree cooler climate.

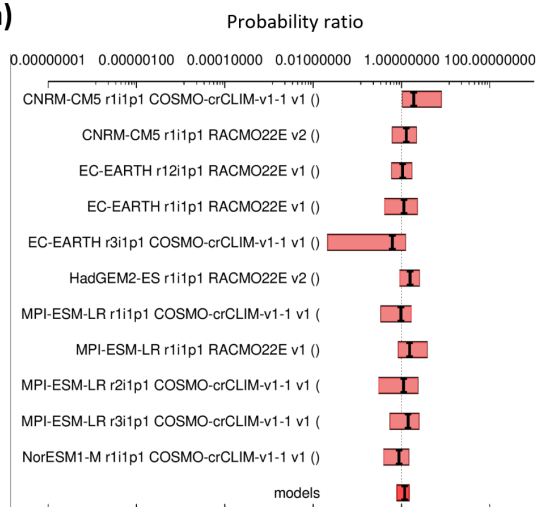
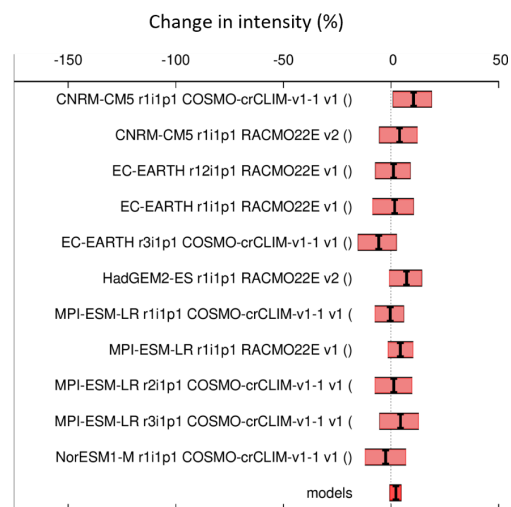
(a)**(b)**

Figure 23: Synthesis of (a) probability ratios and (b) intensity changes when comparing the 2-day maximum October precipitation that occurred in 2023 with a 0.8 degree warmer climate.

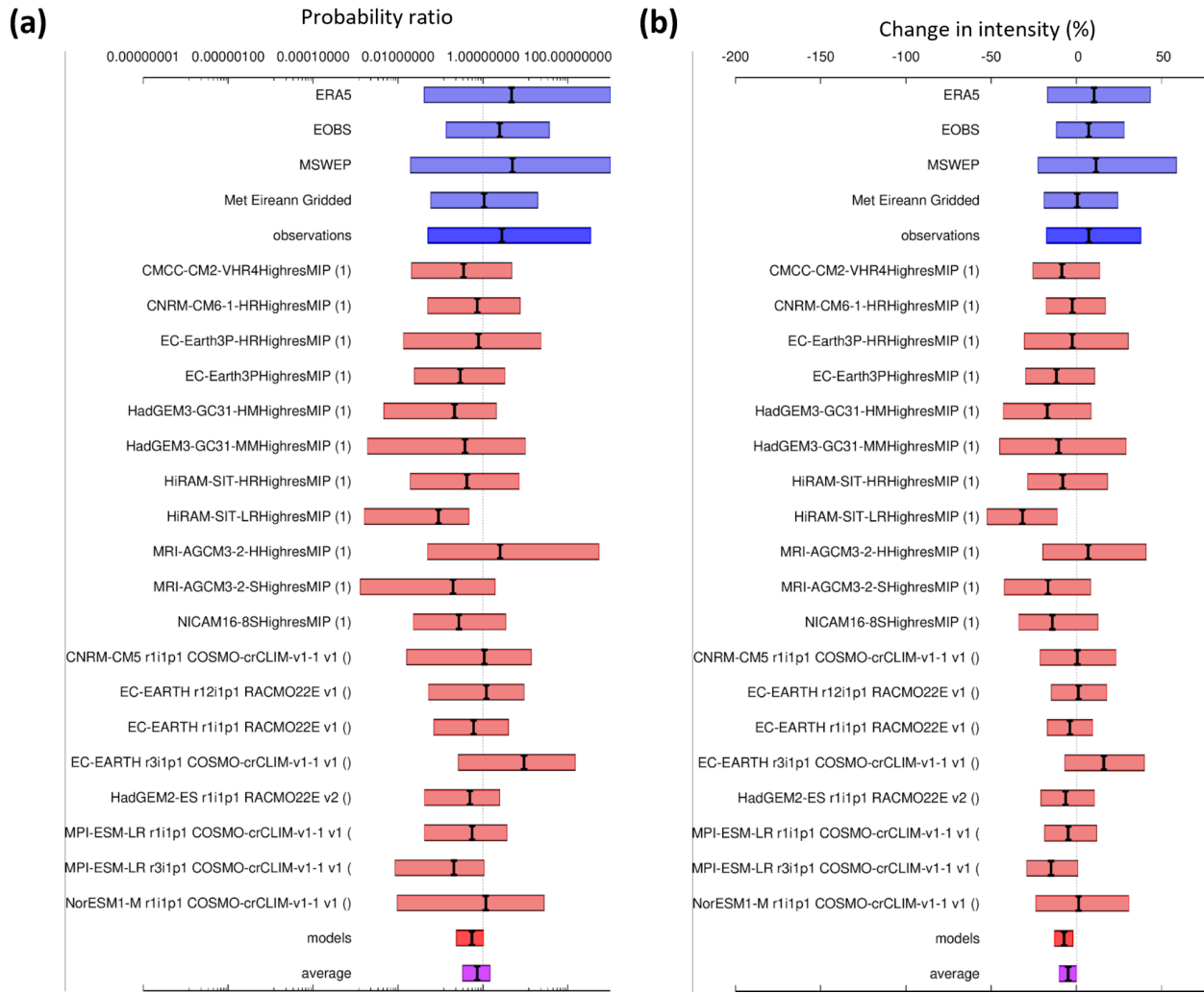


Figure 24: Synthesis of (a) probability ratios and (b) intensity changes when comparing the July-September precipitation that occurred in 2023 with a 1.2 degree cooler climate.

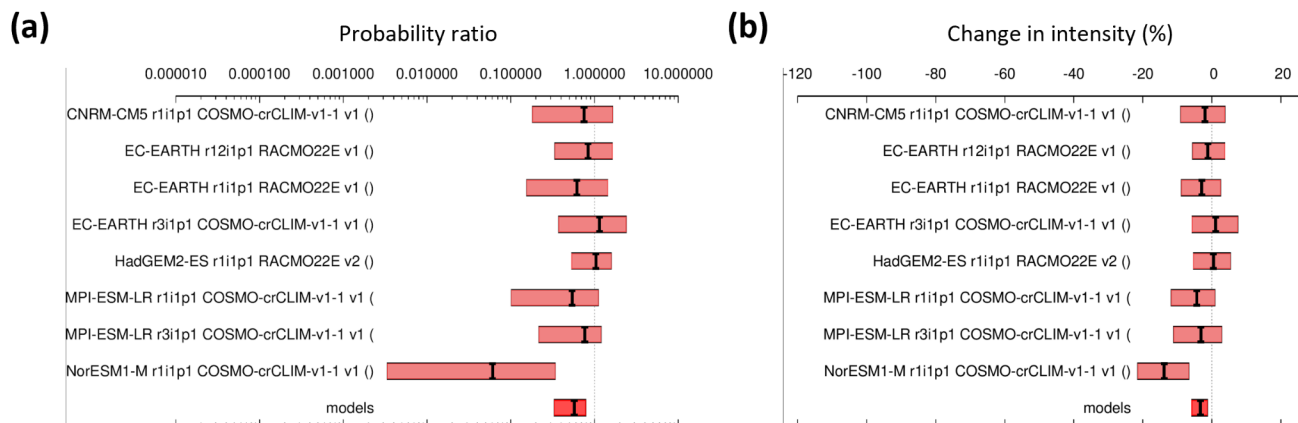


Figure 25: Synthesis of (a) probability ratios and (b) intensity changes when comparing the July-September precipitation that occurred in 2023 with a 0.8 degree warmer climate.

3.1.4 Rainfall hazard synthesis

3.1.4.1 October 2-day max

| Time period (data type) | | Probability ratio (95% CI) | Intensity change (%) (95% CI) |
|-------------------------|--------------|----------------------------|-------------------------------|
| Past-Present | Observations | 6.38 (0.77 - 4740) | 34.3 (-6.89 - 90.6) |
| | Models | 1.86 (0.94 - 6.02) | 9.21 (1.61 - 16.9) |
| | Synthesis | 2.23 (1.22 - 7.34) | 12.6 (5.22 - 20.0) |
| Present-Future | Models only | 1.18 (0.80 - 1.47) | 2.28 (-0.44 - 4.59) |

Table 6: Summary of results presented in Figs 22 & 23, including observed and modelled present and future changes in 2-day October maximum rainfall. Statistically significant increases in probability and intensity are highlighted in dark blue, while non-significant increases are highlighted in light blue.

For the event in the present day, the synthesis result shows robust increases in both likelihood and intensity. An event such as occurred in 2023 has become around 120% more likely and results in around 13% more rainfall, which is above the expected Clausius-Clapeyron scaling. Although models give a significantly lower magnitude of change with an associated lower uncertainty (due in part to a greater volume of data), both models and observations agree on the sign of change. The resultant synthesis is also significant, suggesting high confidence in this result. At 2 degrees, a further 20% increase in probability is expected and a small increase in intensity. However, both results include no further change, and the results rely upon models only that are shown to give lower magnitude changes than are observed to date, so while confidence in the likelihood and magnitude both further increasing is high, confidence in the precise quantification is low.

3.1.4.2 July-September accumulation

| Time period (data type) | | Probability ratio (95% CI) | Intensity change (%) (95% CI) |
|-------------------------|--------------|----------------------------|-------------------------------|
| Past-Present | Observations | 2.82 (0.05 - 345) | 7.35 (-17.4 - 37.8) |
| | Models | 0.55 (0.24 - 1.02) | -7.18 (-12.8 - -2.11) |
| | Synthesis | 0.73 (0.34 - 1.45) | -4.80(-10.0 - 0.09) |
| Present-Future | Models only | 0.57 (0.33 - 0.78) | -3.33 (-5.77 - -1.33) |

Table 7: Summary of results presented in Figs 24 & 25, including observed and modelled present and future changes in July-September rainfall. Statistically significant decreases in probability and intensity are highlighted in dark orange, while non-significant decreases are highlighted in light orange, and non-significant increases are highlighted in light blue.

The synthesis results for July-September accumulations show a decrease by around 30% in likelihood and 5% in rainfall totals. However, both the probability ratio and intensity results encompass no change. In addition, observations and models disagree on the sign of change, meaning these results are of very low confidence. At 2 degrees, a further 40% decrease in probability is simulated and a small decrease in intensity, which are both significant. Given the disagreement between models and observations to the present day, this result remains very low confidence.

4. Full Hazard Synthesis and Discussion

The region around Midleton is remarkably well-instrumented, enabling a forensic examination of the causes of the event in a manner that would be desirable in all event attribution studies. Analysis of this range of tidal, hydrometric, precipitation and satellite data along with a commissioned report from Arup (2023a,b) leaves little doubt as to the causes of the flooding in Midleton: fluvial flows from the river catchments draining into Cork Harbour at Midleton. These fluvial flows can be extremely well modelled by a simple regression on 2-day and prior 3 months precipitation. Or, in simpler terms, the wet late summer / early autumn pre-conditioned the river catchments such that the two-day extreme precipitation from Storm Babet in October led to extensive flooding across Midleton. The tidal gauge records provide the final piece of the puzzle. The flooding peaked at spring low tide and there was minimal storm surge. The low sea levels enabled the flood waters to escape quickly and, most likely, averted an even more catastrophic outcome for Midleton. Even with these favourable conditions, peak tidal residuals were of comparable magnitude to the largest storm surges observed in Cork Harbour.

This analysis led to an attribution of the extreme rainfall associated with the event, both the 2-day accumulations on 17-18th October, and the July-September totals. Using a multi-method multi-model probabilistic attribution, the climate change influence on these events were calculated and synthesised, along with confidence levels in these results and the reasoning behind this (Table 8).

| Event and time period | | Rainfall attribution - best estimate change | | Confidence level | |
|-----------------------|----------------|---------------------------------------------|------------------|---------------------------------------------|-----------------------------------------------------------------------------------------------------------------------------------------------------------------------------------------------|
| | | Probability (%) | Intensity (%) | Value | Reasoning |
| 2-day | Past-present | Increase (+ 123%) | Increase (+ 13%) | High | Stations, gridded observations and models agree on sign of change, results are significant. |
| | Present-future | Increase (+ 18%) | Increase (+ 2%) | High in sign, Low in precise quantification | Model agreement and physical understanding give high confidence in sign. For quantification, models give a lower magnitude than all observations to present, and results are non-significant. |
| 3-month | Past-present | Decrease (- 27%) | Decrease (- 5%) | Very low | Models and observations disagree on sign of change, results non-significant. |
| | Present-future | Decrease (- 33%) | Decrease (- 3%) | Very low | Models and observations disagree on sign of change, results are significant. |

Table 8: Summary of the best estimates for the rainfall attribution statements, along with qualitative confidence levels based on levels of agreement across models and observations and statistical significance of the results.

The greatest confidence result is for the 2-day extremes to present. This is based on strong agreement across models and observations, both gridded products and station time series. The present-future result is based purely on model projections, which are shown to have a substantially lower trend than the models. The quantitative result therefore cannot have confidence greater than low, and we expect that the result for this is a conservative one. Nonetheless, due to the strong trend to date and physical understanding based on Clausius-Clapeyron scaling, confidence in the qualitative result, that the likelihood and intensity of 2-day extreme rainfall is increasing further with future warming, is high. Meanwhile, confidence is very low across the board for the 3-month accumulations. This is because there is a fundamental disagreement between models and observations on the direction of change and the dominant physical drivers of changes to precipitation on this timescale are less clear. While all the gridded datasets and 3 of the 5 stations show increases (resulting in a net increase for the observational synthesis), 2 stations and the models all show decreases with warming. This means that our final messages contain no strong statements on the influence of climate change on the preconditioning July-September rainfall.

The seemingly contradictory findings on the July-September cumulative rainfall attribution between observation-based and model-based estimates could arise from one or more of three non-exclusive causes:

1. The real-world climate that we have lived and experienced could, by chance, have had a series of wet July-September periods arising from internal climate system variability and not from external climate system drivers. Interestingly, some individual model simulations (Figures 22 & 24) included in the multi-model ensemble do show agreement with the observed results, lending some credence to this possibility (although it could also arise because those models pick up important physical processes lacking in remaining models). Furthermore, 2023 was an extreme year for North Atlantic Sea Surface Temperatures (SSTs) with an extreme marine heatwave off Irish waters ([McCarthy et al., 2023](#)). [Berthou et al. \(submitted\)](#) argue that an expected result of this would be a period of sustained excess precipitation over adjacent land regions by up to 20%. Given the extreme nature of the marine heatwave in 2023, both this and its associated impacts on rainfall are unlikely to be adequately captured within the multi-model ensemble of opportunity used herein.
2. There could exist common systematic biases in all the observational products. Given that many arise from the same set of rainfall gauges common biases in these cannot be ruled out. However: i) the reanalyses precipitation estimates are independent of these gauge measurements; and ii) the gauge data have been extensively used and tested for homogeneity in several analyses which have found no evidence of data inhomogeneities ([Ryan et al., 2021](#)).
3. The climate model simulations assessed could suffer from (largely) common biases via missing key processes important in JAS precipitation in the region and leading to historical simulations (and potentially future projections) that are not consistent with the real-world climate system in this region and for this precipitation diagnostic.

It is beyond the scope of this study to further investigate and disentangle this issue. We do note, however, that it would be valuable to improve understanding of this issue and any ramifications for projections of future changes in the region.

There is also a less stark and statistically insignificant, but still potentially important, difference in 2-day October extreme precipitation results between models and observations. Models exhibit, on average, lesser increases in both probability and intensity than observation-based estimates over the historical period. However, observation-based estimates have very considerable spread. The consensus estimate is therefore dominated by the model-based evidence which exhibits lower spread. Similar to the preceding discussion, if the model ensemble as a whole exhibits common limitations then: i) the attributable increase in event probability and intensity could be higher; and ii) the assessed future changes in probability and intensity could also be underestimated.

5. Conclusions

5.1 Final results

The Middleton flooding event in October 2023 resulted from a 2-day precipitation extreme event coming on top of 3 months of above average precipitation accumulations. This led to the most

extreme river heights measured on the Owenacurra river since at least 2000 when 15-minute resolution gauge reporting commenced. The flood event was likely mitigated by hitting at a spring low tide, which permitted fast draining of the fluvial flood into Cork Harbour. As noted in the Midleton Flood Relief scheme [documentation](#), Midleton is prone to both fluvial and storm surge related flooding. The risk is that in future such events might coincide, and fluvial and marine impacts may reinforce each other rather than partially cancel each other out as was likely the case in October 2023.

Our analysis shows with high confidence that the 2-day precipitation event has been made more than twice as likely and 13% more intense. With lower confidence in a 2-degree warmer world the 2-day extreme event would be made a further 20% more likely and 2% more intense than today. The analysis is much less certain in terms of the three-month accumulations with very low confidence that the totals observed in 2023 have been made less likely and the expected cumulative total precipitation has become lower. Observations and models for the historical period paint overall diverging narratives for late summer / early autumn seasonal accumulations and more work is required in future to unpick this. The overall conclusion is that climate change has made the event more likely and more severe, with expected increase with further warming, and the risk of worse events in the present given the co-occurrence of high tides and/or storm surge.

5.2 Broader Implications

As noted in [Volume 1 of Ireland's Climate Change Assessment](#), published in early 2024, there would be considerable value in investing in and sustaining a national operational event attribution capability for Ireland. This study has served as a case study of how such a service could be undertaken and add value to national policy making and planning moving forwards. Firstly, the analysis served to highlight, in a way hitherto neglected, how the tides helped to reduce the impact of the event. Secondly, the quantified assessment of the human contribution to both 2-day and 3-month precipitation can now be used to stress test, and if necessary modify, the plans for the future Midleton relief scheme. Thirdly, the findings have relevance to at least Cork and likely broader parts of southern Ireland so may inform other planned flood protection schemes, translated appropriately to the specific contexts. Finally, the multi-disciplinary analysis highlighted the value of sustained observations to understand climate risk and resilience. It was the combination of measurements from across numerous government agencies together with the various skills of the interdisciplinary team that allowed the event to be so well understood.

At a broader level, forensic attribution studies such as this one highlight where, whether and to what degree the current level of warming is having impacts on communities and property through its influence on extreme weather. This provides evidence towards an accurate and nuanced picture of the costs of climate change to date for the public and policymakers alike, it provides a platform for future risk assessment based on plausible events, and can inform both adaptation to and mitigation of further climate changes. The applicability of hazard-based attribution studies such as this is greatly improved with consideration of factors contributing to the exposure and vulnerability of those affected, such as levels of insurance, early warning systems, development decisions (past and future), and access to vital services. Given that the extreme rainfall leading to flooding is only going to increase with further warming, the availability and affordability of insurance for homes and businesses alike will be a

crucial determinant of risk going forwards ([Irish Independent, 2024](#)).

5.3 Further work

To close, there are several further investigations or dataset developments which could improve our knowledge arising from this brief study as follows:

Spatiotemporal domain - Our analysis was necessarily limited to a specific subset of the year and to County Cork. It would be informative and useful to generalise the analysis across the entire calendar year and other counties or regions. This could begin by looking at the different flood events evident in the historical record around the coast and key basins, noting that any flood protection scheme needs to protect against all flood types. It may be that the human contributions have substantial seasonal variations and thus increase or decrease risk across the year compared to that implied for specifically October events in the present study.

Coastal and fluvial compound flooding events – The simultaneous occurrence of high rainfall and storm surge, or even high tide, particularly as sea levels rise, can result in far greater flood extents than either one occurring in isolation. In this case, the low spring tide meant that there was no need for a quantitative analysis of the effects of either storm surge or tidal lock impacts for this particular event. However, there is no guarantee that Midleton will not at some point in the future confront both extreme fluvial flooding and tidal lock exacerbated by storm surge. Analysis over all European coastlines suggests that such compound events are becoming significantly more likely due to climate change around the west coasts of Ireland and Great Britain ([Bevacqua et al., 2019](#)). We would note that our methodologies would require considerable extension to properly handle such a compound extreme event and assessing the potential human contributions to it.

Storyline approach to attribution – Extreme weather attribution refers to a suite of methods that can be used to probe the influence of anthropogenic climate change. This study employed a highly probabilistic framing, considering changes in the likelihood of any sources of rainfall, not simply storms like Babet. This gives a comprehensive view of extreme rainfall probability but may result in relatively high uncertainties due to a lack of understanding of how atmospheric dynamics leading to storms like Babet are changing. To probe the direct influence of additional heat on a given storm system, a highly conditional or ‘storyline’ approach could be taken, which involves understanding how the event evolved.

Storm Babet itself was an extratropical cyclone laden with moisture having arisen off the Iberian Peninsula some days earlier. Total column precipitable water values of 30-50mm were widespread within the storm system. The highly anomalously warm North Atlantic basin in 2023 could have played an important role in these elevated precipitable water values. The storm was long-lived and slow moving leading to large precipitation accumulations centred in east Cork / west Waterford, and these properties may have been affected by warming in different ways. Therefore, such an investigation could begin with the occurrence of Storm Babet itself, and perturbing SSTs in the basin to values with and without human-caused warming, then measuring how the accumulated rainfall from the storm changed. In this way, the thermodynamic influence of climate change can be understood more directly and with lower uncertainty, with the caveat that the more uncertain

dynamical changes are assumed to be unchanging, and that the result is applicable only to storms like Babet.

Differences between observations and models - There is a need to unpick the disagreements between the observed and multi-model ensemble behaviour for rainfall changes. This is most stark for the July-September seasonal accumulation but also potentially pertains to a lesser extent for the 2-day extreme events. For the latter, the weaker trend in Met Éireann gridded data than other gridded observational and reanalysis products is of particular interest. To test these differences, it would be necessary to undertake in-depth analysis, testing multiple hypotheses (such as those set out in section 4), to understand whether these differences point to issues in observations, models, or simply internal variability, noting that these explanations are not mutually exclusive.

Land use change data - The analysis of the contribution of land use changes was limited by the lack of availability of high-quality land-use change information across multiple decades. Much of the change in land-use in Ireland occurred in the mid-20th Century, associated with land drainage improvement works. This precedes the availability of satellite-based products. These satellite products are also relatively coarse resolution and may not adequately resolve changes across the relatively small river catchments. These limitations significantly limited our analysis of land-use change. A national land-use change dataset at high resolution and covering a longer period would have provided valuable information. Furthermore, projections of potential future land use changes in various development scenarios would enable proactive risk assessment.

Risk assessment – as mentioned in section 5.2, risk is the product of hazard with the exposure and vulnerability to that hazard. Ultimately, this study was triggered because of the impacts of the event on people in Midleton. It is the effect of climate change on these impacts that would be the most useful result for all the potential applications of attribution studies. However, it is challenging and time-consuming to conduct a quantitative study to attribute impacts directly. This involves following the causal chain of events from meteorology to specific impacts, requiring a cascade of models of different kinds that creates compounding uncertainties. Nonetheless, even simple assessments of exposure and vulnerability as separate factors aid in contextualising climate change as one driver of risk among others, both human and natural, and therefore highlight where efforts can return the greatest benefits to those affected.

Data availability

Almost all data are available via the Climate Explorer.

For Met Éireann data please visit www.met.ie or contact Ciara Ryan (ciara.ryan@met.ie)

Ringaskiddy tide gauge data is available from <https://waterlevel.ie/0000019069/>

Bailick Road tide gauge data is available from <https://waterlevel.ie/0000019165/0001/>

River flow in Owenacurra at Ballyedmond can be downloaded from

<https://epawebapp.epa.ie/hydronet/#19020>

UKMO synoptic analysis charts retrieved from

<https://www.wetterzentrale.de/en/reanalysis.php?map=1&model=bra&var=45>

Acknowledgements

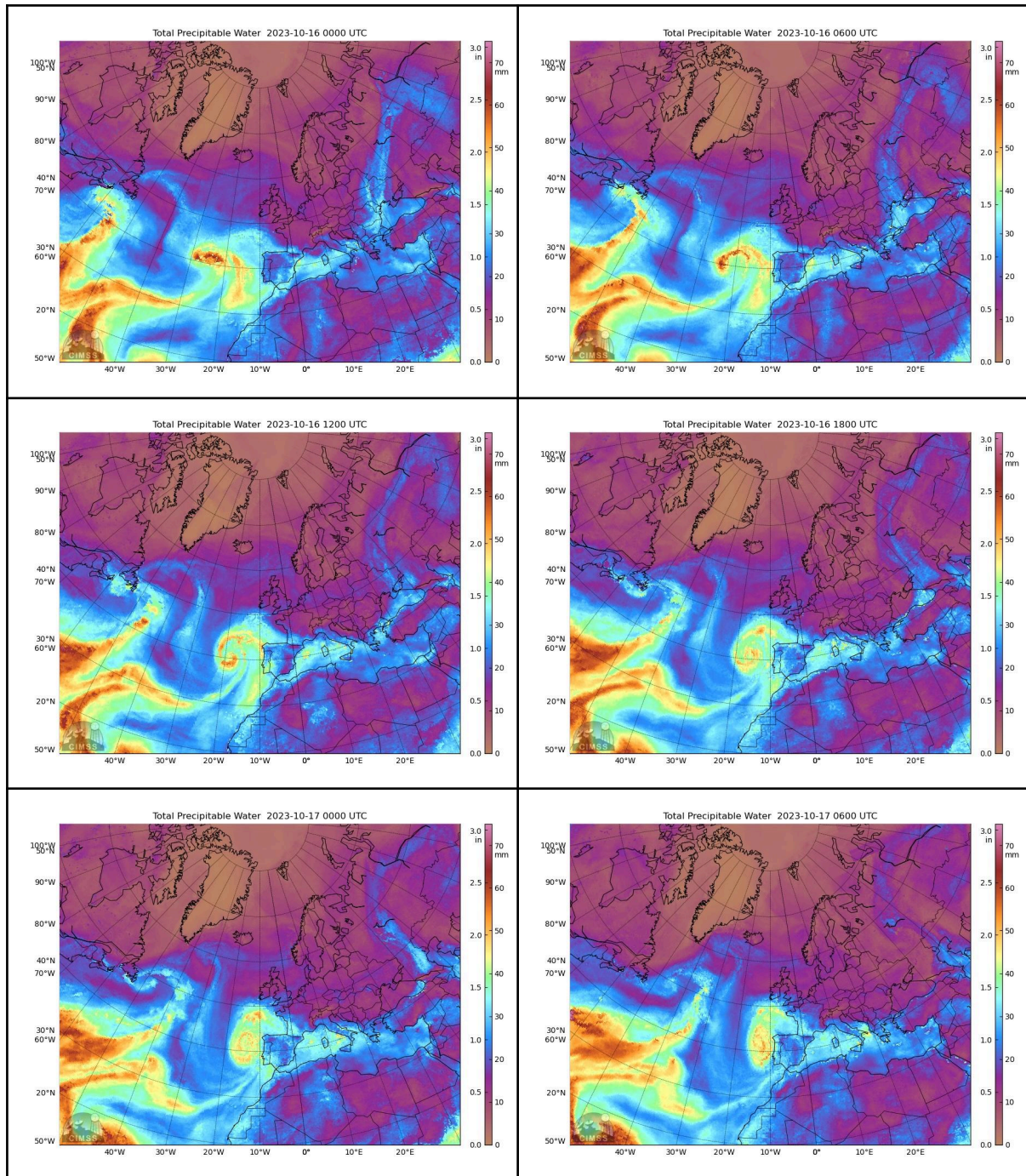
CM and NC acknowledge funding from the Irish Environmental Protection Agency via the HydroDARE: Detection and Attribution of Change in Hydrological Series project (2022-CE-1132).

Development of the MIMIC-TPW2 product is supported by the JPSS Risk Reduction Program and the Office of Naval Research.

References

All references are given as hyperlinks in the text.

Supplementary material



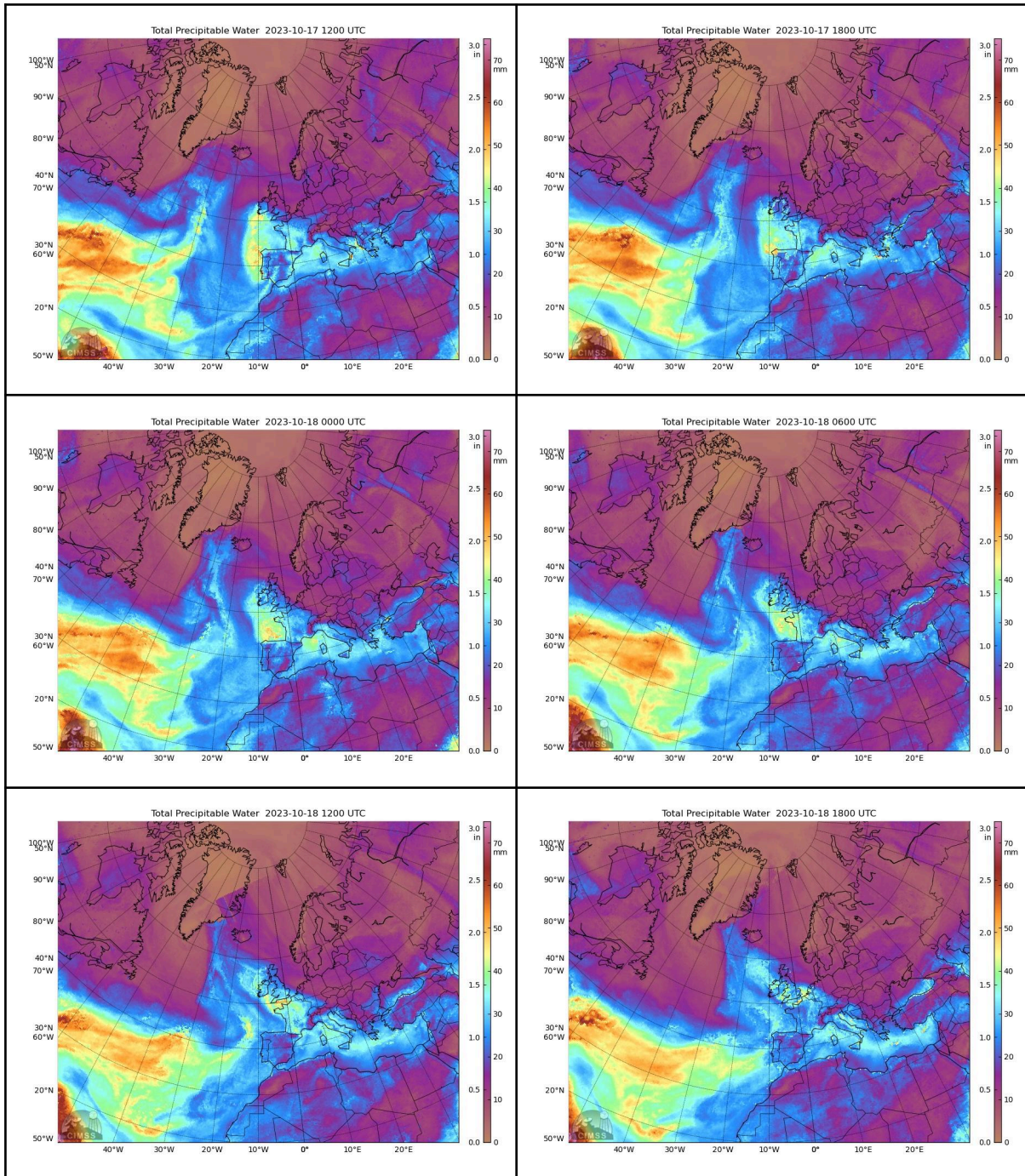


Figure S1. 6 hourly snapshots of Total Precipitable Water estimates from 00 UTC on 16/10/23 until 18 UTC on 18/10/23 covering the period of the analysis herein. Sourced from the [MIMIC-TPW2 product](#) from CIMMS, University of Wisconsin-Madison.

Model evaluation

HighResMIP

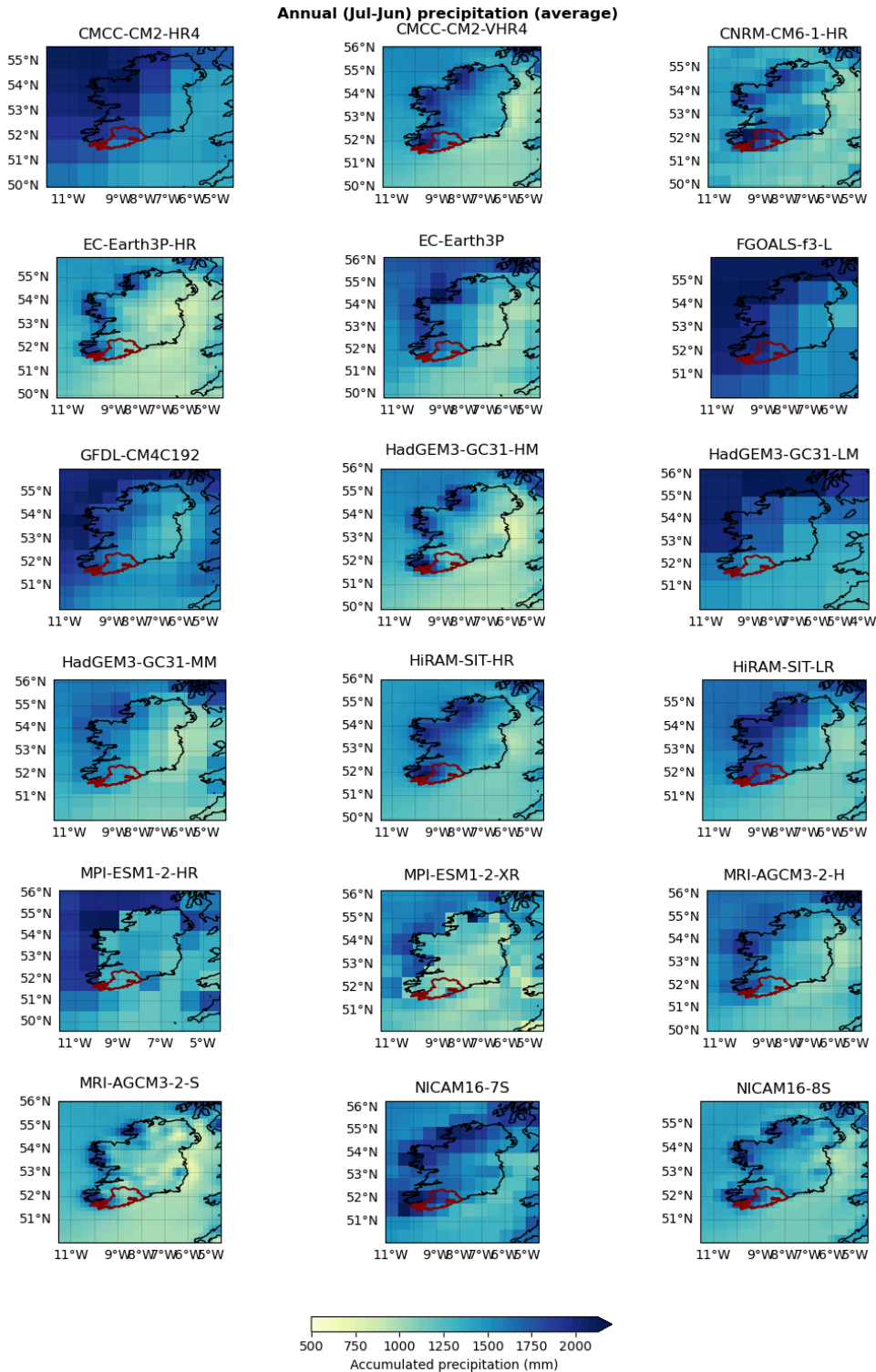


Figure S2: Spatial pattern of annual precipitation in each of the HighResMIP ensemble members. County Cork is highlighted in red.

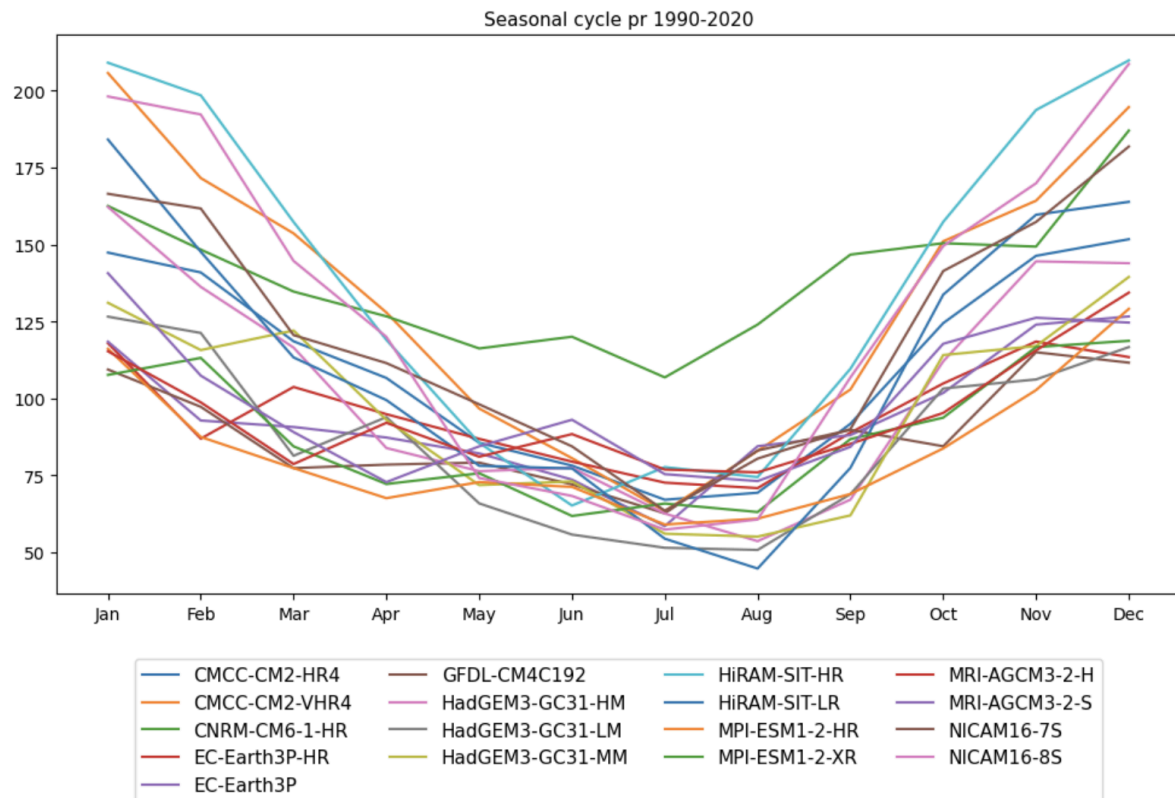
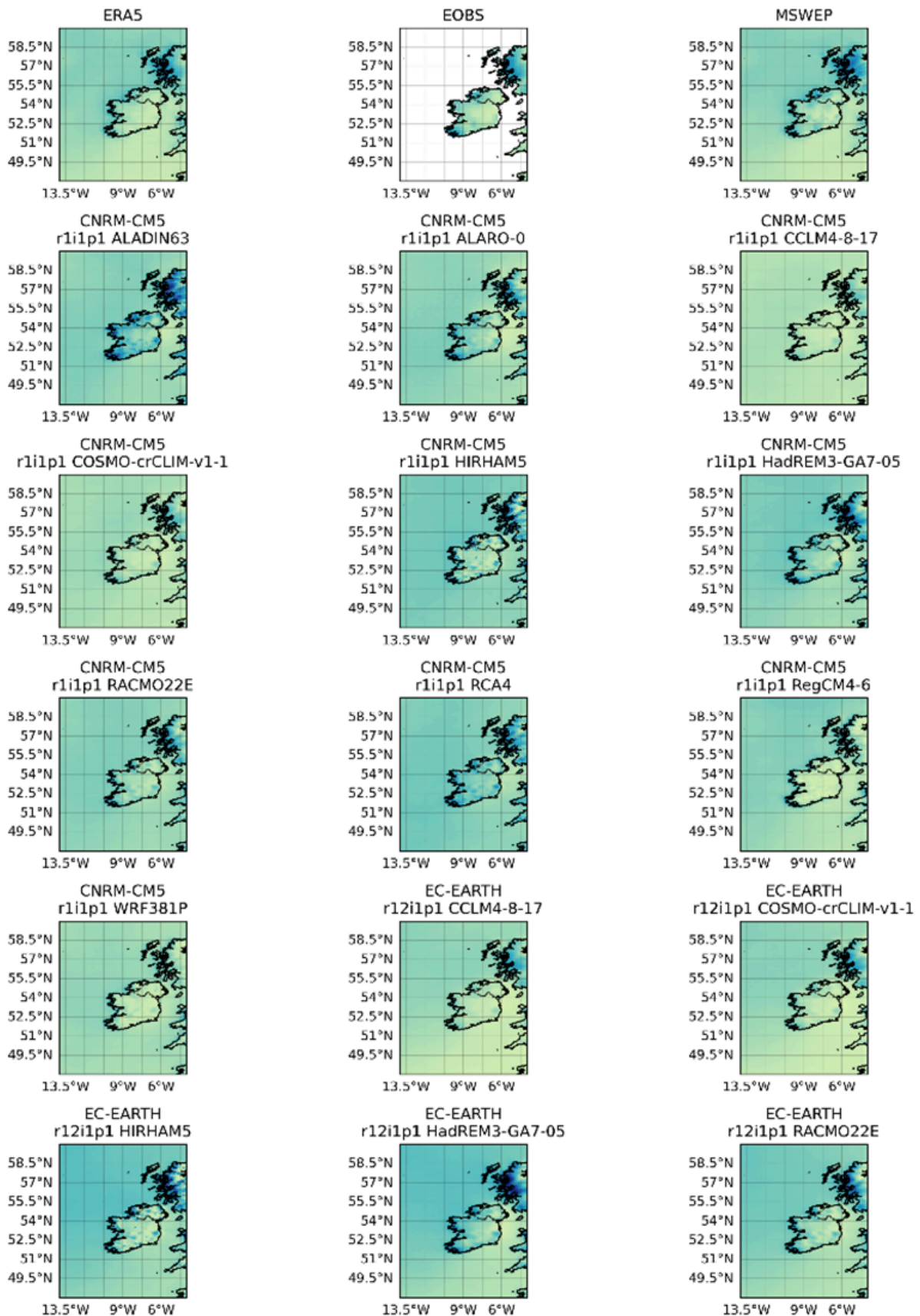
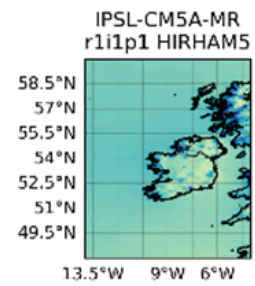
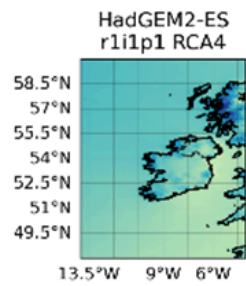
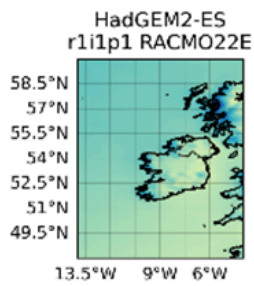
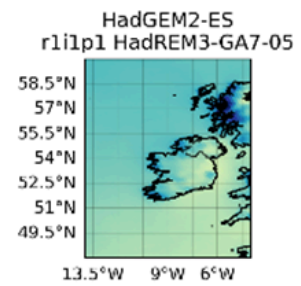
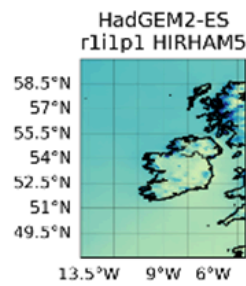
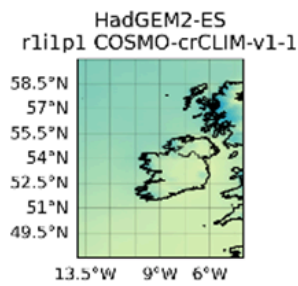
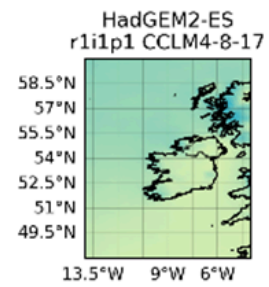
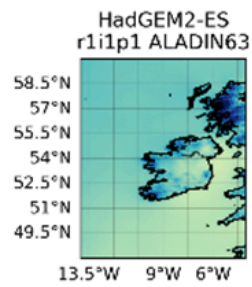
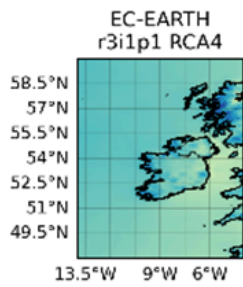
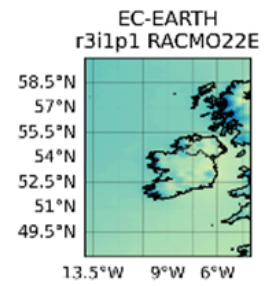
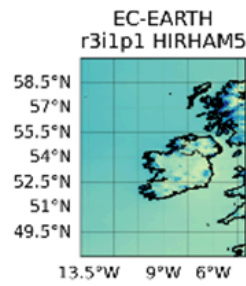
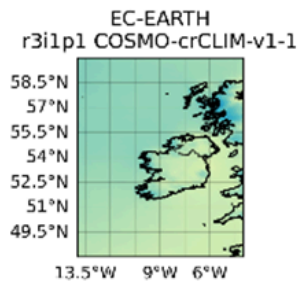
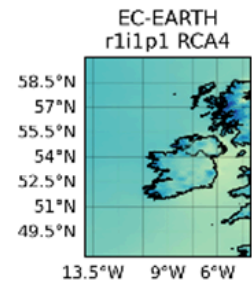
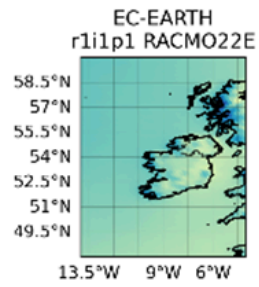
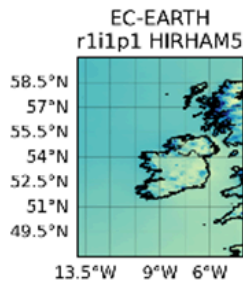
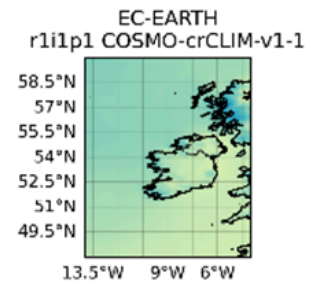
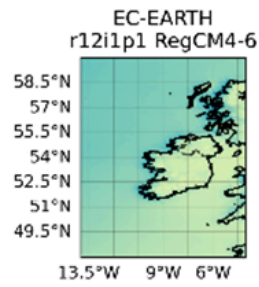
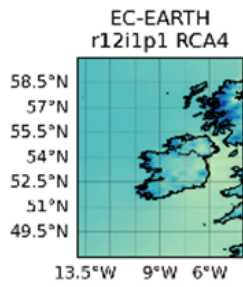


Figure S3: Seasonal cycle of annual precipitation in each of the HighResMIP ensemble members.

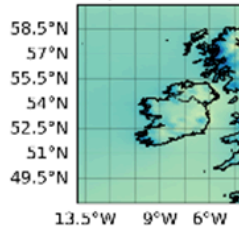
EURO-CORDEX

Spatial pattern of annual precipitation in ERA5 & CORDEX

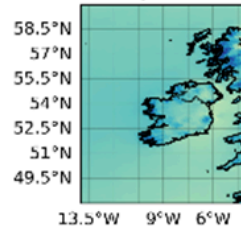




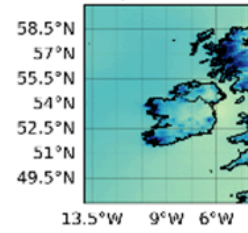
IPSL-CM5A-MR
r1i1p1 RACMO22E



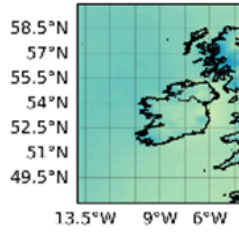
IPSL-CM5A-MR
r1i1p1 RCA4



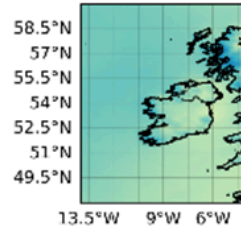
MPI-ESM-LR
r1i1p1 ALADIN63



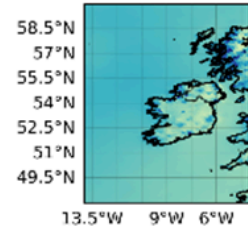
MPI-ESM-LR
r1i1p1 CCLM4-8-17



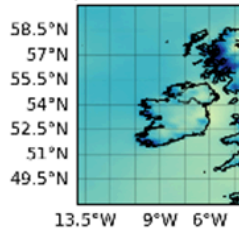
MPI-ESM-LR
r1i1p1 COSMO-crCLIM-v1-1



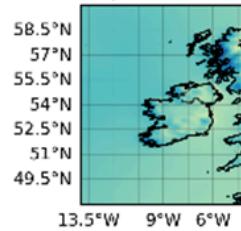
MPI-ESM-LR
r1i1p1 HIRHAM5



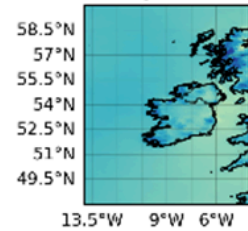
MPI-ESM-LR
r1i1p1 HadREM3-GA7-05



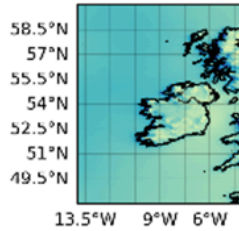
MPI-ESM-LR
r1i1p1 RACMO22E



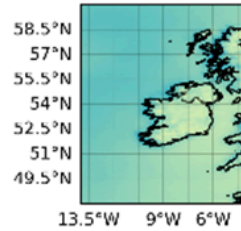
MPI-ESM-LR
r1i1p1 RCA4



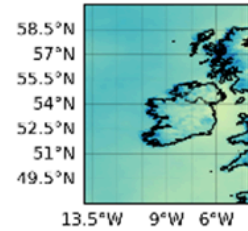
MPI-ESM-LR
r1i1p1 REMO2009



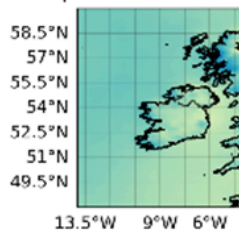
MPI-ESM-LR
r1i1p1 RegCM4-6



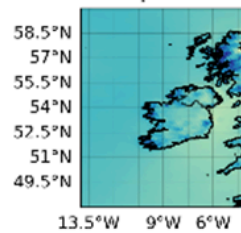
MPI-ESM-LR
r1i1p1 WRF361H



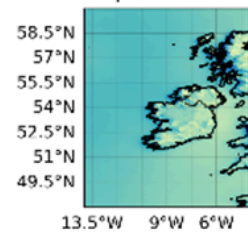
MPI-ESM-LR
r2i1p1 COSMO-crCLIM-v1-1



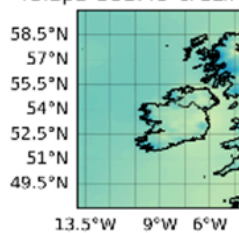
MPI-ESM-LR
r2i1p1 RCA4



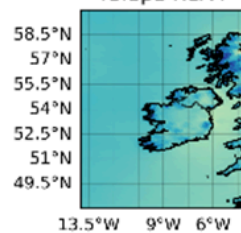
MPI-ESM-LR
r2i1p1 REMO2009



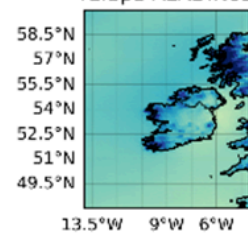
MPI-ESM-LR
r3i1p1 COSMO-crCLIM-v1-1



MPI-ESM-LR
r3i1p1 RCA4



NorESM1-M
r1i1p1 ALADIN63



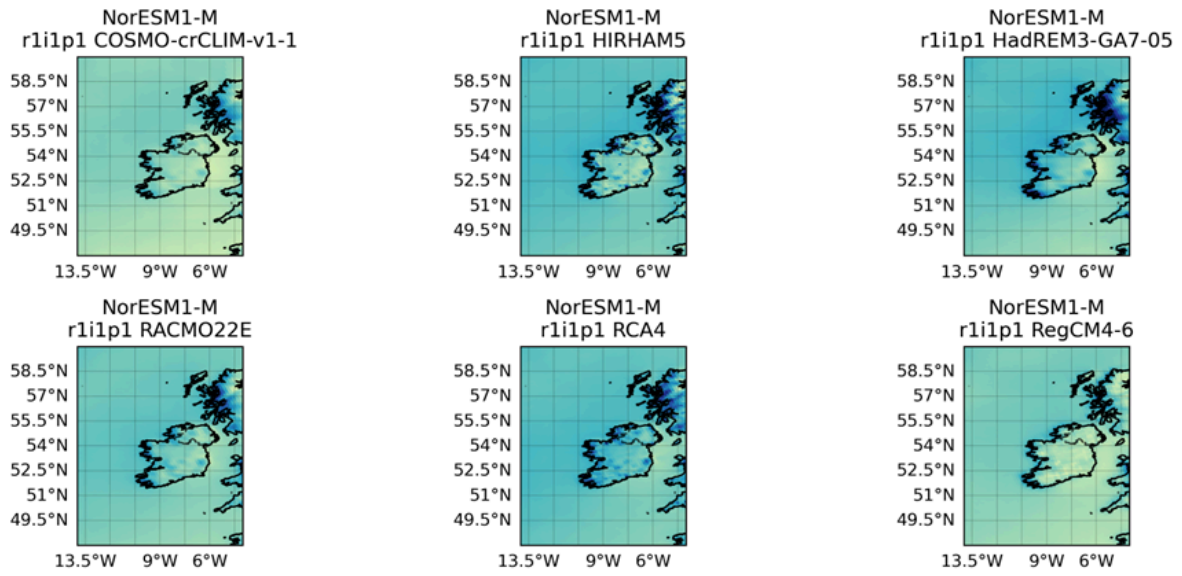
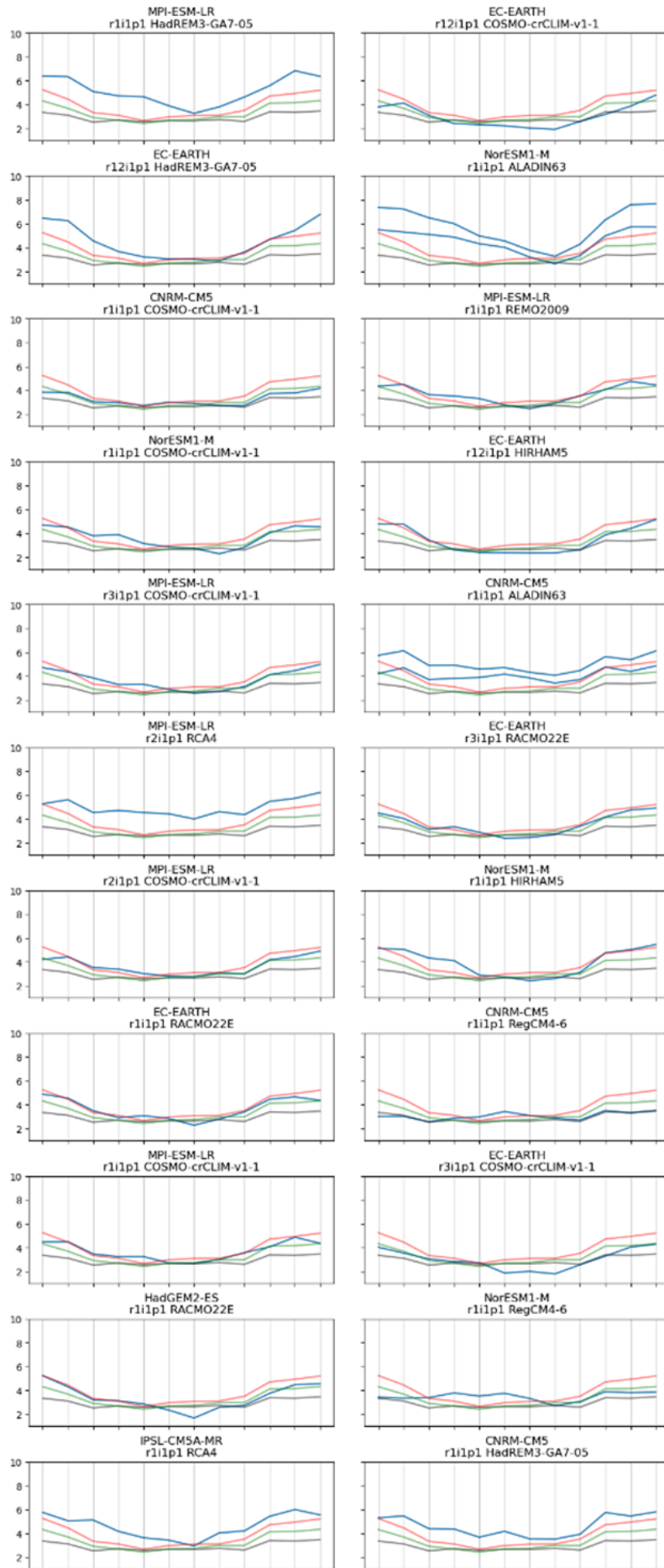
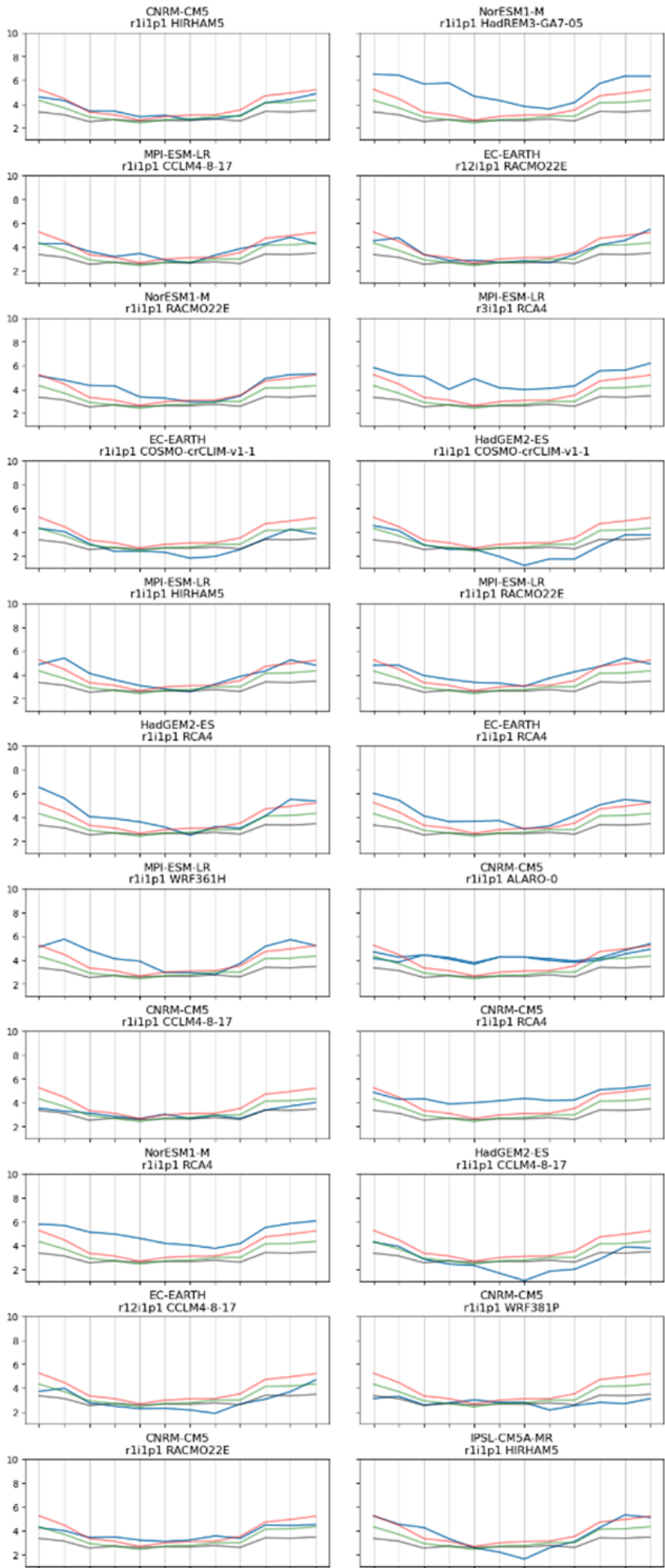


Figure S4: Spatial pattern of annual precipitation in each of the HighResMIP ensemble members.

Seasonal cycle of precipitation over study region in ERA5 (black), EObs (red), MSWEP (green) & CORDEX (blue)





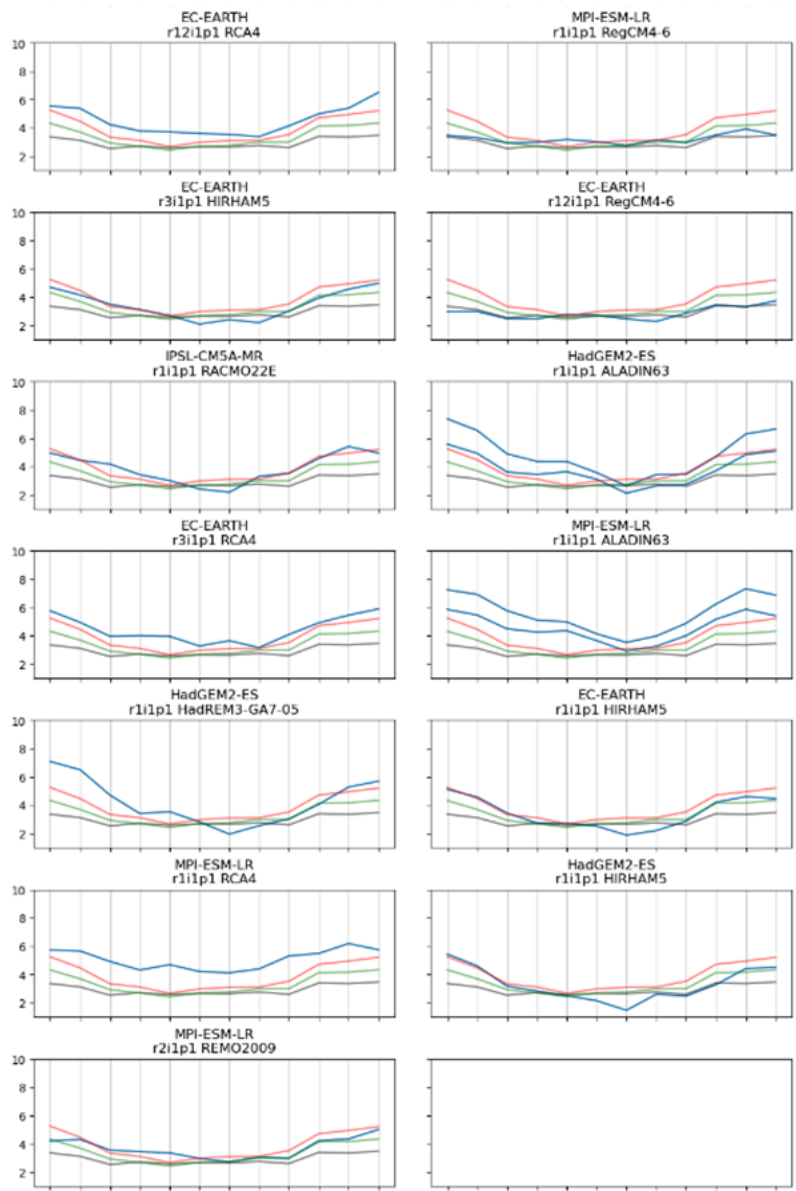


Figure S5: Seasonal cycle of annual precipitation over County Cork in each of the EURO-CORDEX ensemble members (blue), compared to observational datasets ERA5 (black), E-OBS (red), and MSWEP (green).

Validation tables

October 2-day maximum precipitation

| Model / Observations | Seasonal cycle | Spatial pattern | Dispersion | Shape parameter | Conclusion |
|-------------------------------|----------------|-----------------|-------------------------|--------------------------|------------|
| ERA5 | | | 0.399 (0.320 ... 0.456) | -0.012 (-0.19 ... 0.17) | |
| EOBS | | | 0.411 (0.345 ... 0.464) | 0.074 (-0.075 ... 0.23) | |
| MSWEP | | | 0.367 (0.270 ... 0.442) | -0.10 (-0.49 ... 0.11) | |
| Met Eireann Gridded | | | 0.384 (0.317 ... 0.439) | -0.037 (-0.22 ... 0.088) | |
| | | | | | |
| HighResMIP | | | | | |
| CMCC-CM2-HR4HighresMIP (1) | reasonable | bad | 0.343 (0.241 ... 0.411) | 0.12 (-0.17 ... 0.34) | bad |
| CMCC-CM2-VHR4HighresMIP (1) | reasonable | good | 0.279 (0.218 ... 0.322) | 0.097 (-0.25 ... 0.33) | reasonable |
| CNRM-CM6-1-HRHighresMIP (1) | good | reasonable | 0.394 (0.282 ... 0.464) | -0.13 (-0.42 ... 0.13) | reasonable |
| EC-Earth3P-HRHighresMIP (1) | reasonable | reasonable | 0.472 (0.346 ... 0.565) | -0.10 (-0.57 ... 0.23) | reasonable |
| EC-Earth3PHighresMIP (1) | reasonable | reasonable | 0.468 (0.296 ... 0.553) | 0.022 (-0.18 ... 0.31) | reasonable |
| GFDL-CM4C192HighresMIP (1) | reasonable | bad | 0.565 (0.444 ... 0.651) | -0.077 (-0.44 ... 0.29) | bad |
| HadGEM3-GC31-HMHighresMIP (1) | reasonable | good | 0.515 (0.371 ... 0.647) | -0.091 (-0.33 ... 0.13) | reasonable |
| HadGEM3-GC31-LMHighresMIP (1) | reasonable | bad | 0.406 (0.301 ... 0.492) | -0.27 (-0.63 ... -0.078) | bad |
| HadGEM3-GC31-MMHighresMIP (1) | reasonable | reasonable | 0.437 (0.316 ... 0.503) | 0.20 (-0.22 ... 1.0) | reasonable |

| | | | | | |
|-----------------------------------------|------------|------------|----------------------------|----------------------------|------------|
| HiRAM-SIT-HRHighresMIP (1) | reasonable | good | 0.308 (0.231 ... 0.363) | -0.12 (-0.57 ... 0.12) | reasonable |
| HiRAM-SIT-LRHighresMIP (1) | reasonable | good | 0.339 (0.265 ... 0.385) | -0.061 (-0.32 ... 0.21) | reasonable |
| MPI-ESM1-2-HRHighresMIP (1) | reasonable | bad | 0.446 (0.330 ... 0.532) | -0.10 (-0.58 ... 0.056) | bad |
| MPI-ESM1-2-XRHighresMIP (1) | reasonable | reasonable | 0.333 (0.255 ... 0.388) | -0.025 (-0.35 ... 0.33) | reasonable |
| MRI-AGCM3-2-HHighresMIP (1) | reasonable | reasonable | 0.442 (0.327 ... 0.561) | -0.21 (-0.61 ... 0.081) | reasonable |
| MRI-AGCM3-2-SHighresMIP (1) | reasonable | reasonable | 0.517 (0.367 ... 0.659) | -0.29 (-0.65 ... -0.15) | reasonable |
| NICAM16-7SHighresMIP (1) | reasonable | bad | 0.313 (0.226 ... 0.373) | 0.095 (-0.14 ... 0.41) | bad |
| NICAM16-8SHighresMIP (1) | reasonable | reasonable | 0.445 (0.327 ... 0.560) | -0.21 (-0.53 ... 0.024) | reasonable |
| CORDEX | | | | | |
| CNRM-CM5_r1i1p1_CCLM4-8-17_v1 () | good | reasonable | 0.364 (0.248 ... 0.434) | 0.049 (-0.21 ... 0.30) | reasonable |
| CNRM-CM5_r1i1p1_COSMO-crCLIM-v1-1_v1 () | good | good | 0.424 (0.305 ... 0.536) | -0.11 (-1.0 ... 0.13) | good |
| CNRM-CM5_r1i1p1_HadREM3-GA7-05_v2 () | reasonable | good | 0.503 (0.360 ... 0.608) | -0.038 (-0.53 ... 0.12) | reasonable |
| CNRM-CM5_r1i1p1_HIRHAM5_v2 () | good | reasonable | 0.464 (0.345 ... 0.548) | -0.086 (-0.37 ... 0.10) | reasonable |
| CNRM-CM5_r1i1p1_RACMO22E_v2 () | good | good | 0.437 (0.336 ... 0.506) | -0.092 (-0.35 ... 0.22) | good |
| CNRM-CM5_r1i1p1_RCA4_v1 () | bad | good | 0.358 (0.283 ... 0.407) | 0.091 (-0.26 ... 0.38) | bad |
| CNRM-CM5_r1i1p1_RegCM4-6_v2 () | reasonable | bad | 0.412 (0.293 ... 0.507) | -0.073 (-0.40 ... 0.25) | bad |
| CNRM-CM5_r1i1p1_WRF381P_v2 () | bad | bad | 0.467 (0.345 ... 0.550) | -0.071 (-0.49 ... 0.30) | bad |

| | | | | | |
|-------------------------------------------|------------|------------|----------------------------|-----------------------------|------------|
| EC-EARTH_r12i1p1_CCLM4-8-17_v1 () | good | reasonable | 0.405 (0.311 ... 0.486) | -0.18 (-1.0 ... -0.013) | reasonable |
| EC-EARTH_r12i1p1_COSMO-crCLIM-v1-1_v1 () | good | reasonable | 0.372 (0.284 ... 0.431) | -0.16 (-0.50 ... 0.094) | reasonable |
| EC-EARTH_r12i1p1_HadREM3-GA7-05_v1 () | reasonable | reasonable | 0.394 (0.302 ... 0.463) | 0.13 (-0.11 ... 0.40) | reasonable |
| EC-EARTH_r12i1p1_HIRHAM5_v1 () | good | reasonable | 0.360 (0.221 ... 0.442) | -0.022 (-0.29 ... 0.52) | reasonable |
| EC-EARTH_r12i1p1_RACMO22E_v1 () | good | good | 0.337 (0.249 ... 0.408) | -0.18 (-0.61 ... -0.029) | good |
| EC-EARTH_r12i1p1_RCA4_v1 () | reasonable | good | 0.346 (0.247 ... 0.419) | -0.088 (-0.35 ... 0.19) | reasonable |
| EC-EARTH_r12i1p1_RegCM4-6_v1 () | reasonable | reasonable | 0.403 (0.303 ... 0.490) | -0.11 (-0.41 ... 0.079) | reasonable |
| EC-EARTH_r1i1p1_COSMO-crCLIM-v1-1_v1 () | reasonable | good | 0.467 (0.356 ... 0.544) | -0.12 (-0.51 ... 0.096) | reasonable |
| EC-EARTH_r1i1p1_HIRHAM5_v1 () | reasonable | reasonable | 0.442 (0.317 ... 0.528) | 0.027 (-0.36 ... 0.22) | reasonable |
| EC-EARTH_r1i1p1_RACMO22E_v1 () | good | good | 0.439 (0.336 ... 0.505) | -0.12 (-0.48 ... 0.16) | good |
| EC-EARTH_r1i1p1_RCA4_v1 () | reasonable | good | 0.412 (0.289 ... 0.504) | -0.038 (-0.54 ... 0.18) | reasonable |
| EC-EARTH_r3i1p1_COSMO-crCLIM-v1-1_v1 () | good | good | 0.345 (0.255 ... 0.405) | -0.084 (-0.47 ... 0.31) | good |
| EC-EARTH_r3i1p1_HIRHAM5_v2 () | good | reasonable | 0.382 (0.293 ... 0.435) | 0.11 (-0.33 ... 0.58) | reasonable |
| EC-EARTH_r3i1p1_RACMO22E_v1 () | good | good | 0.269 (0.208 ... 0.312) | -0.18 (-0.48 ... 0.18) | reasonable |
| EC-EARTH_r3i1p1_RCA4_v1 () | reasonable | good | 0.336 (0.240 ... 0.400) | -0.19 (-0.50 ... 0.14) | reasonable |
| HadGEM2-ES_r1i1p1_CCLM4-8-17_v1 () | bad | reasonable | 0.549 (0.392 ... 0.736) | -0.69 (-1.1 ... -0.077) | bad |
| HadGEM2-ES_r1i1p1_COSMO-crCLIM-v1-1_v1 () | bad | reasonable | 0.615 (0.481 ... 0.712) | 0.040 (-0.62 ... 0.35) | bad |

| | | | | | |
|-------------------------------------------|------------|------------|---------------------------|-------------------------|------------|
| HadGEM2-ES_r1i1p1_HadREM3-GA7-05_v1 () | reasonable | good | 0.550 (0.426 ... 0.651) | -0.078 (-0.37 ... 0.14) | reasonable |
| HadGEM2-ES_r1i1p1_HIRHAM5_v2 () | reasonable | reasonable | 0.447 (0.333 ... 0.512) | 0.20 (-0.14 ... 0.66) | reasonable |
| HadGEM2-ES_r1i1p1_RACMO22E_v2 () | good | good | 0.432 (0.323 ... 0.540) | -0.30 (-1.1 ... 0.14) | good |
| HadGEM2-ES_r1i1p1_RCA4_v1 () | reasonable | good | 0.466 (0.327 ... 0.560) | 0.069 (-0.58 ... 0.44) | reasonable |
| IPSL-CM5A-MR_r1i1p1_HIRHAM5_v1 () | reasonable | reasonable | 0.349 (0.253 ... 0.412) | -0.054 (-0.49 ... 0.15) | reasonable |
| IPSL-CM5A-MR_r1i1p1_RACMO22E_v1 () | reasonable | good | 0.332 (0.212 ... 0.411) | -0.13 (-0.58 ... 0.41) | reasonable |
| IPSL-CM5A-MR_r1i1p1_RCA4_v1 () | reasonable | good | 0.345 (0.270 ... 0.393) | 0.076 (-0.29 ... 0.35) | reasonable |
| MPI-ESM-LR_r1i1p1_CCLM4-8-17_v1 () | good | good | 0.260 (0.172 ... 0.319) | -0.15 (-0.41 ... 0.22) | reasonable |
| MPI-ESM-LR_r1i1p1_COSMO-crCLIM-v1-1_v1 () | good | good | 0.307 (0.240 ... 0.424) | -0.24 (-1.1 ... 0.076) | good |
| MPI-ESM-LR_r1i1p1_HadREM3-GA7-05_v1 () | bad | good | 0.298 (0.211 ... 0.367) | -0.15 (-0.61 ... 0.15) | bad |
| MPI-ESM-LR_r1i1p1_HIRHAM5_v1 () | good | reasonable | 0.305 (0.235 ... 0.367) | 0.054 (-0.60 ... 0.29) | reasonable |
| MPI-ESM-LR_r1i1p1_RACMO22E_v1 () | good | good | 0.305 (0.194 ... 0.371) | -0.044 (-0.30 ... 0.34) | good |
| MPI-ESM-LR_r1i1p1_RCA4_v1a () | bad | good | 0.282 (0.220 ... 0.328) | 0.048 (-0.41 ... 0.38) | bad |
| MPI-ESM-LR_r1i1p1_RegCM4-6_v1 () | reasonable | bad | 0.298 (0.223 ... 0.350) | -0.011 (-0.35 ... 0.28) | bad |
| MPI-ESM-LR_r1i1p1_REMO2009_v1 () | good | bad | 0.331 (0.240 ... 0.394) | 0.024 (-0.32 ... 0.38) | bad |
| MPI-ESM-LR_r1i1p1_WRF361H_v1 () | bad | good | 0.165 (0.00334 ... 0.308) | 0.38 (-1.1 ... 5.2) | bad |
| MPI-ESM-LR_r2i1p1_COSMO-crCLIM-v1-1_v1 () | good | good | 0.438 (0.308 ... 0.540) | -0.16 (-0.45 ... 0.062) | good |

| | | | | | |
|-------------------------------------------|------------|------------|----------------------------|-----------------------------|------------|
| MPI-ESM-LR_r2i1p1_RCA4_v1 () | bad | good | 0.423 (0.299 ... 0.509) | 0.017 (-0.33 ... 0.30) | bad |
| MPI-ESM-LR_r2i1p1_REMO2009_v1 () | good | bad | 0.462 (0.288 ... 0.569) | 0.042 (-0.28 ... 0.62) | bad |
| MPI-ESM-LR_r3i1p1_COSMO-crCLIM-v1-1_v1 () | good | good | 0.273 (0.203 ... 0.330) | 0.050 (-0.27 ... 0.25) | good |
| MPI-ESM-LR_r3i1p1_RCA4_v1 () | reasonable | reasonable | 0.313 (0.237 ... 0.371) | 0.098 (-0.14 ... 0.28) | reasonable |
| NorESM1-M_r1i1p1_COSMO-crCLIM-v1-1_v1 () | good | good | 0.330 (0.259 ... 0.388) | 0.029 (-0.49 ... 0.47) | good |
| NorESM1-M_r1i1p1_HadREM3-GA7-05_v1 () | bad | reasonable | 0.349 (0.249 ... 0.414) | -0.0076 (-0.32 ... 0.30) | bad |
| NorESM1-M_r1i1p1_HIRHAM5_v3 () | good | reasonable | 0.364 (0.277 ... 0.420) | 0.026 (-0.33 ... 0.32) | reasonable |
| NorESM1-M_r1i1p1_RACMO22E_v1 () | reasonable | good | 0.344 (0.252 ... 0.409) | -0.0011 (-0.60 ... 0.38) | reasonable |
| NorESM1-M_r1i1p1_RCA4_v1 () | bad | good | 0.367 (0.273 ... 0.436) | -0.037 (-0.40 ... 0.17) | bad |
| NorESM1-M_r1i1p1_RegCM4-6_v1 () | bad | reasonable | 0.212 (0.157 ... 0.252) | 0.085 (-0.20 ... 0.39) | bad |

Table S1: Evaluation results of the climate models considered for attribution analysis of the October maximum 2-day precipitation over the study region. The table consists of qualitative assessments of the seasonal cycles and spatial patterns, the sigma and shape parameters from fitting a GEV distribution that shifts with GMST, and the conclusion of the evaluation process. Models are coloured according to the valuation, orange for 'bad', yellow for 'reasonable', and green for 'good'. For HighResMIP, all reasonable models are included in the synthesis, whereas for CORDEX only good models are included.

July-September accumulated precipitation

| Model / Observations | Seasonal cycle | Spatial pattern | Dispersion | Conclusion |
|-------------------------------|----------------|-----------------|-------------------------|------------|
| ERA5 | | | 0.314 (0.257 ... 0.356) | |
| EOBS | | | 0.297 (0.253 ... 0.331) | |
| MSWEP | | | 0.271 (0.213 ... 0.313) | |
| Met Eireann Gridded | | | 0.281 (0.239 ... 0.313) | |
| | | | | |
| HighResMIP | | | | |
| CMCC-CM2-HR4HighresMIP (1) | reasonable | bad | 0.253 (0.163 ... 0.304) | bad |
| CMCC-CM2-VHR4HighresMIP (1) | reasonable | good | 0.234 (0.182 ... 0.269) | reasonable |
| CNRM-CM6-1-HRHighresMIP (1) | good | reasonable | 0.240 (0.183 ... 0.280) | reasonable |
| EC-Earth3P-HRHighresMIP (1) | reasonable | reasonable | 0.356 (0.275 ... 0.411) | reasonable |
| EC-Earth3PHighresMIP (1) | reasonable | reasonable | 0.307 (0.234 ... 0.372) | reasonable |
| GFDL-CM4C192HighresMIP (1) | reasonable | bad | 0.248 (0.187 ... 0.298) | bad |
| HadGEM3-GC31-HMHighresMIP (1) | reasonable | good | 0.375 (0.302 ... 0.431) | reasonable |
| HadGEM3-GC31-LMHighresMIP (1) | reasonable | bad | 0.329 (0.264 ... 0.379) | bad |
| HadGEM3-GC31-MMHighresMIP (1) | reasonable | reasonable | 0.412 (0.303 ... 0.490) | reasonable |
| HiRAM-SIT-HRHighresMIP (1) | reasonable | good | 0.312 (0.247 ... 0.362) | reasonable |

| | | | | |
|-----------------------------------------|------------|------------|----------------------------|------------|
| HIRAM-SIT-LRHighresMIP (1) | reasonable | good | 0.390 (0.306 ... 0.446) | reasonable |
| MPI-ESM1-2-HRHighresMIP (1) | reasonable | bad | 0.212 (0.175 ... 0.239) | bad |
| MPI-ESM1-2-XRHighresMIP (1) | reasonable | bad | 0.275 (0.228 ... 0.315) | bad |
| MRI-AGCM3-2-HHighresMIP (1) | reasonable | reasonable | 0.254 (0.197 ... 0.293) | reasonable |
| MRI-AGCM3-2-SHighresMIP (1) | reasonable | reasonable | 0.315 (0.246 ... 0.353) | reasonable |
| NICAM16-7SHighresMIP (1) | reasonable | bad | 0.290 (0.218 ... 0.353) | bad |
| NICAM16-8SHighresMIP (1) | reasonable | reasonable | 0.332 (0.264 ... 0.381) | reasonable |
| CORDEX | | | | |
| CNRM-CM5_r1i1p1_CCLM4-8-17_v1 () | good | reasonable | 0.234 (0.193 ... 0.261) | reasonable |
| CNRM-CM5_r1i1p1_COSMO-crCLIM-v1-1_v1 () | good | good | 0.242 (0.188 ... 0.280) | good |
| CNRM-CM5_r1i1p1_HadREM3-GA7-05_v2 () | reasonable | good | 0.246 (0.197 ... 0.283) | reasonable |
| CNRM-CM5_r1i1p1_HIRHAM5_v2 () | good | reasonable | 0.238 (0.178 ... 0.283) | reasonable |
| CNRM-CM5_r1i1p1_RACMO22E_v2 () | good | good | 0.182 (0.144 ... 0.211) | bad |
| CNRM-CM5_r1i1p1_RCA4_v1 () | bad | good | 0.215 (0.169 ... 0.245) | bad |
| CNRM-CM5_r1i1p1_RegCM4-6_v2 () | reasonable | bad | 0.209 (0.162 ... 0.242) | bad |
| CNRM-CM5_r1i1p1_WRF381P_v2 () | bad | bad | 0.225 (0.173 ... 0.260) | bad |
| EC-EARTH_r12i1p1_CCLM4-8-17_v1 () | good | reasonable | 0.337 (0.258 ... 0.389) | reasonable |

| | | | | |
|-------------------------------------------|------------|------------|-------------------------|------------|
| EC-EARTH_r12i1p1_COSMO-crCLIM-v1-1_v1 () | good | reasonable | 0.336 (0.253 ... 0.382) | reasonable |
| EC-EARTH_r12i1p1_HadREM3-GA7-05_v1 () | reasonable | reasonable | 0.300 (0.236 ... 0.339) | reasonable |
| EC-EARTH_r12i1p1_HIRHAM5_v1 () | good | reasonable | 0.266 (0.213 ... 0.302) | reasonable |
| EC-EARTH_r12i1p1_RACMO22E_v1 () | good | good | 0.242 (0.197 ... 0.271) | good |
| EC-EARTH_r12i1p1_RCA4_v1 () | reasonable | good | 0.251 (0.197 ... 0.286) | reasonable |
| EC-EARTH_r12i1p1_RegCM4-6_v1 () | reasonable | reasonable | 0.241 (0.192 ... 0.279) | reasonable |
| EC-EARTH_r1i1p1_COSMO-crCLIM-v1-1_v1 () | reasonable | good | 0.289 (0.223 ... 0.338) | reasonable |
| EC-EARTH_r1i1p1_HIRHAM5_v1 () | reasonable | reasonable | 0.267 (0.188 ... 0.327) | reasonable |
| EC-EARTH_r1i1p1_RACMO22E_v1 () | good | good | 0.213 (0.165 ... 0.249) | good |
| EC-EARTH_r1i1p1_RCA4_v1 () | reasonable | good | 0.245 (0.186 ... 0.289) | reasonable |
| EC-EARTH_r3i1p1_COSMO-crCLIM-v1-1_v1 () | good | good | 0.309 (0.251 ... 0.352) | good |
| EC-EARTH_r3i1p1_HIRHAM5_v2 () | good | reasonable | 0.238 (0.180 ... 0.280) | reasonable |
| EC-EARTH_r3i1p1_RACMO22E_v1 () | good | good | 0.202 (0.165 ... 0.227) | reasonable |
| EC-EARTH_r3i1p1_RCA4_v1 () | reasonable | good | 0.166 (0.118 ... 0.209) | bad |
| HadGEM2-ES_r1i1p1_CCLM4-8-17_v1 () | bad | reasonable | 0.356 (0.278 ... 0.414) | bad |
| HadGEM2-ES_r1i1p1_COSMO-crCLIM-v1-1_v1 () | bad | reasonable | 0.384 (0.310 ... 0.443) | bad |
| HadGEM2-ES_r1i1p1_HadREM3-GA7-05_v1 () | reasonable | good | 0.277 (0.221 ... 0.319) | reasonable |

| | | | | |
|-------------------------------------------|------------|------------|-----------------------------|------------|
| HadGEM2-ES_r1i1p1_HIRHAM5_v2 () | reasonable | reasonable | 0.280 (0.230 ... 0.317) | reasonable |
| HadGEM2-ES_r1i1p1_RACMO22E_v2 () | good | good | 0.271 (0.219 ... 0.315) | good |
| HadGEM2-ES_r1i1p1_RCA4_v1 () | reasonable | good | 0.266 (0.215 ... 0.303) | reasonable |
| IPSL-CM5A-MR_r1i1p1_HIRHAM5_v1 () | reasonable | reasonable | 0.230 (0.174 ... 0.281) | reasonable |
| IPSL-CM5A-MR_r1i1p1_RACMO22E_v1 () | reasonable | good | 0.197 (0.149 ... 0.234) | reasonable |
| IPSL-CM5A-MR_r1i1p1_RCA4_v1 () | reasonable | good | 0.189 (0.143 ... 0.228) | reasonable |
| MPI-ESM-LR_r1i1p1_CCLM4-8-17_v1 () | good | good | 0.210 (0.150 ... 0.261) | reasonable |
| MPI-ESM-LR_r1i1p1_COSMO-crCLIM-v1-1_v1 () | good | good | 0.231 (0.170 ... 0.275) | good |
| MPI-ESM-LR_r1i1p1_HadREM3-GA7-05_v1 () | bad | good | 0.230 (0.162 ... 0.277) | bad |
| MPI-ESM-LR_r1i1p1_HIRHAM5_v1 () | good | reasonable | 0.194 (0.145 ... 0.235) | reasonable |
| MPI-ESM-LR_r1i1p1_RACMO22E_v1 () | good | good | 0.184 (0.131 ... 0.218) | reasonable |
| MPI-ESM-LR_r1i1p1_RCA4_v1a () | bad | good | 0.160 (0.113 ... 0.193) | bad |
| MPI-ESM-LR_r1i1p1_RegCM4-6_v1 () | reasonable | bad | 0.208 (0.163 ... 0.238) | bad |
| MPI-ESM-LR_r1i1p1_REMO2009_v1 () | good | bad | 0.215 (0.153 ... 0.260) | bad |
| MPI-ESM-LR_r1i1p1_WRF361H_v1 () | bad | good | 0.144 (0.0865 ... 0.176) | bad |
| MPI-ESM-LR_r2i1p1_COSMO-crCLIM-v1-1_v1 () | good | good | 0.196 (0.148 ... 0.241) | reasonable |
| MPI-ESM-LR_r2i1p1_RCA4_v1 () | bad | good | 0.154 (0.117 ... 0.185) | bad |

| | | | | |
|-----------------------------------------------|------------|------------|----------------------------|------------|
| MPI-ESM-LR_r2i1p1_REMO2009_v1 () | good | bad | 0.213 (0.165 ... 0.246) | bad |
| MPI-ESM-LR_r3i1p1_COSMO-crCLIM-v1-1_v 1 () | good | good | 0.307 (0.244 ... 0.354) | good |
| MPI-ESM-LR_r3i1p1_RCA4_v1 () | reasonable | reasonable | 0.196 (0.147 ... 0.228) | reasonable |
| NorESM1-M_r1i1p1_COSMO-crCLIM-v1-1_v 1 () | good | good | 0.294 (0.232 ... 0.340) | good |
| NorESM1-M_r1i1p1_HadREM3-GA7-05_v1 () | bad | reasonable | 0.271 (0.217 ... 0.310) | bad |
| NorESM1-M_r1i1p1_HIRHAM5_v3 () | good | reasonable | 0.217 (0.159 ... 0.264) | reasonable |
| NorESM1-M_r1i1p1_RACMO22E_v1 () | reasonable | good | 0.189 (0.149 ... 0.221) | reasonable |
| NorESM1-M_r1i1p1_RCA4_v1 () | bad | good | 0.192 (0.147 ... 0.230) | bad |
| NorESM1-M_r1i1p1_RegCM4-6_v1 () | bad | reasonable | 0.204 (0.163 ... 0.230) | bad |

Table S2: Evaluation results of the climate models considered for attribution analysis of the July-September accumulated precipitation over the study region. The table consists of qualitative assessments of the seasonal cycles and spatial patterns, the dispersion parameter from fitting a Gaussian distribution that shifts with GMST, and the conclusion of the evaluation process. Models are coloured according to the valuation, orange for 'bad', yellow for 'reasonable', and green for 'good'. For HighResMIP, all reasonable models are included in the synthesis, whereas for CORDEX only good models are included.